~~The risky middle~~ High probability of ~~the road - probabilities of~~ triggering climate tipping points under current policies modestly amplified by Amazon dieback and ~~how they increase due to tipping points within the Earth's carbon cycle~~ permafrost thaw

Jakob Deutloff[1, 2, 3], Hermann Held[4], and Timothy M Lenton[1]

[1]Global Systems Institute, University of Exeter, Exeter, UK.
[2]Center for Earth System Research and Sustainability (CEN), Meteorological Institute, Universität Hamburg, Hamburg, Germany.
[3]International Max Planck Research School on Earth System Modelling (IMPRS-ESM), Hamburg, Germany.
[4]Research Unit Sustainability and Global Change and Center for Earth System Research and Sustainability, Universität Hamburg, Germany.

Correspondence: Jakob Deutloff (jakob.deutloff@mpimet.mpg.de)

Abstract. We investigate the probabilities of triggering climate tipping points under various shared socioeconomic pathways (SSPs), and how they are altered by including the additional carbon emissions that could arise from tipping points within the Earth's carbon cycle. Crossing of a climate tipping point at a threshold level of global mean surface temperature (threshold temperature), would commit the affected subsystem of the Earth to abrupt and largely irreversible changes with negative impacts on human well-being. However, it remains unclear which tipping points would be triggered under the different SSPs, due to uncertainties in the climate sensitivity to anthropogenic greenhouse gas emissions, the threshold temperatures of climate tipping points, and the response of tipping points within the Earth's carbon cycle to global warming. We include those uncertainties in our analysis to derive probabilities of triggering for 16 previously-identified climate tipping points within the Earth system. To conduct our analysis, we use the ~~intermediate~~ reduced complexity climate model FaIR which is coupled to a conceptual model of the tipping processes within the Amazon rainforest and permafrost, which are the two major tipping elements within the Earth's carbon cycle. Uncertainties are propagated by employing a Monte Carlo approach for the construction of large model ensembles. We find that ~~intermediate emission scenarios like~~ SSP2-4.5 ~~are~~, which compares best to the warming trajectory expected from current policies, is highly unsafe with regard to triggering climate tipping points~~, with an average~~. Averaged over all 16 tipping points, the probability of triggering until the year 2500 ~~of 65% . Furthermore, the highest long-term temperature increase among all SSPs caused by carbon emissions from the Amazon and permafrost becomes possible under this scenario with 0.16~~ is 64% under SSP2-4.5, and eight tipping points have a more than 66% probability of getting triggered. The additional warming from abrupt Amazon dieback and permafrost thaw increases the risk for high temperature pathways, but on average remains small compared to the anthropogenic warming. Under SSP2-4.5, abrupt Amazon dieback and permafrost thaw add $0.15°C$ $(0.03 - 0.91°C)$ ~~in 2500, which~~ to global warming in 2500. This additional warming increases the average probability of triggering ~~tipping points~~ until 2500 by 3.3 percent points ~~(pp). This is due to the fact that maximum~~ under SSP2-4.5. Even though this is the maximum triggering probability increase caused by carbon emissions from ~~tipping of~~ the Amazon and

permafrost ~~become possible under this scenario, and they cause most warming when cumulative anthropogenic emissions are lower due to the saturating response of radiative forcing to increasing greenhouse gas concentrations~~among all SSPs, it still remains modest compared to the probability of triggering caused by anthropogenic warming. The risk of triggering climate tipping points is reduced significantly under SSP1-2.6 ~~and even more so under SSP1-1.9,~~ with average probabilities of triggering ~~of 38%and 28% respectively, which are increased by 2.3~~until 2500 of 37%, which is increased by 2.2 ~~pp and 1.1 pp~~ percent points due to carbon emissions from the Amazon and permafrost.

1 Introduction

The term "tipping point" is commonly used to describe a critical threshold in the forcing of a system, at which small additional forcing leads to significant and long-term changes of the system (Lenton et al., 2008). The debate about tipping points in the climate system, referred to as "climate tipping points", has intensified over the past two decades. Increasing numbers of Earth system components have been identified which could possibly exhibit tipping behaviour (e.g. Lenton et al., 2008; Kriegler et al., 2009; Steffen et al., 2018), with 15 candidates being shortlisted in the latest IPCC report (Lee et al., 2021). These Earth system components are referred to as "tipping elements" (TEs) and occur within the biosphere, cryosphere and oceanic or atmospheric circulation (Lenton et al., 2008). The global mean surface temperature (GMST) relative to pre-industrial levels is used as a common metric to describe the forcing of the TEs (Armstrong McKay et al., 2022). This means that a tipping point can be associated with a "threshold temperature" after which the respective TE is expected to exhibit tipping behaviour. There is growing concern about the possible proximity of climate tipping points, as threshold temperatures have been revised to lower levels, with some TEs being at risk of getting "triggered" (crossing of their threshold temperature) at GMST values as low as $1°C$ (Lenton et al., 2019).

In their recent literature synthesis, Armstrong McKay et al. (2022) identify 16 TEs within the Earth system and provide estimates of their threshold temperatures, the characteristic timescales their tipping is assumed to unfold over, and their impact on global warming (Table 1, we will use the abbreviations defined in the table for the different TEs). Building on the definition of TEs by Lenton et al. (2008), Armstrong McKay et al. (2022) distinguish between "global core" and "regional impact" TEs. To qualify as a global core TE, a tipping point has to occur uniformly across a sub-continental scale ($\sim 1000\,\text{km}$) for a subsystem of the Earth. However, if the change in forcing is approximately uniform across a large spatial area, small-scale tipping points can be crossed near-synchronously at a sub-continental scale, which qualifies the affected subsystem as a regional impact TE. Furthermore, global TEs have to contribute significantly to the overall operation mode of the Earth system, while regional impact TEs are required to either contribute significantly to human welfare or to have great value in themselves as unique features of the Earth system.

Since triggering of TEs will negatively affect human welfare, political efforts should be increased to avoid them (Cai et al., 2016). However, it is not straightforward to determine how safe a specific emission scenario is with regard to triggering TEs, since several uncertainties need to be accounted for within this calculation. The climate sensitivity to anthropogenic emissions remains poorly constrained, with a likely range of the equilibrium climate sensitivity to a doubling of atmospheric

55   CO_2 concentrations of $2.5 - 4°C$ (Chen et al., 2021). Furthermore, climate tipping points include uncertainties within their threshold temperatures, timescales, impacts and for some even their existence remains uncertain (Armstrong McKay et al., 2022). Additional uncertainty is introduced by potential interactions of climate tipping points, which tend to destabilize them (Wunderling et al., 2021). Such interactions can be of manifold nature and often involve complex mechanisms. One example are TEs within the Earth's carbon cycle, which have the potential to release large amounts of greenhouse gases (GHGs) and

60   thereby amplify global warming, which in turn increases the probability of triggering other TEs (Steffen et al., 2018).

    In this study, we calculate probabilities of triggering for the 16 TEs that Armstrong McKay et al. (2022) identify within the Earth system, including the uncertainties in climate sensitivities and the threshold temperatures, by employing a Monte Carlo approach (Metropolis et al., 1953). Herewith, we provide an update of the widely used but somewhat outdated probabilities of triggering derived from an expert elicitation conducted by Kriegler et al. (2009). Furthermore, we quantify the additional

65   warming that might arise from TEs within the Earth's carbon cycle and how it increases the probabilities of triggering other TEs.

    TEs with the potential to significantly impact the Earth's carbon cycle include abrupt permafrost thaw or collapse, Amazon rainforest dieback and northern expansion and southern dieback of boreal forest (Armstrong McKay et al., 2022). Since northern expansion and southern dieback of boreal forests ~~are assumed to roughly~~ balance out in terms of global warm-

70   ing~~(Canadell et al., 2021), we focus on permafrost thaw and Amazon dieback .~~, we exclude them from our analysis. The exact nature of this balance remains contested. The latest IPCC report assumes that expansion of boreal forest at their northern edge and dieback of boreal forest accompanied by temperate forest invasion at the southern edge of boreal forests will roughly balance out in terms of carbon emissions (Canadell et al., 2021). On the other hand, Armstrong McKay et al. (2022) argue that the carbon release from southern dieback will be an order of magnitude larger than the sequestered carbon from northern

75   expansion of boreal forests, but the warming would still balance out since it is to first order determined by albedo and evapotranspiration changes (Table 1).

Permafrost thaw can be further subdivided into three distinct processes: gradual ~~thaw,~~ permafrost thaw, which is a threshold-free feedback to global warming~~, abrupt thaw, ~~; abrupt permafrost thaw, which is a regional impact tipping element~~, and collapse, ~~; permafrost collapse, which is a global core tipping element (Armstrong McKay et al., 2022). Since gradual thaw of permafrost,

80   associated with uniform and large-scale deepening of the active layer, is not assumed to include a tipping point, we do not include it in our analysis~~, instead focusing ~~. Instead, we focus on abrupt thaw and collapse of permafrost and Amazon dieback, hereafter referred to as the "carbon tipping elements".

    Abrupt thaw of permafrost occurs regionally but near-synchronously over the permafrost region due to thermokarsts which can affect several meters of permafrost within days to weeks (Turetsky et al., 2019). The emerging landscapes mostly in-

85   clude water-saturated soils (Olefeldt et al., 2016), hence high methane emissions ~~of around 20%~~ from anaerobic respiration of the now accessible soil organic carbon ~~can be expected(Turetsky et al., 2020).~~ must be expected. Around 20% of the carbon emissions from abrupt permafrost thaw are assumed to be released as methane (Turetsky et al., 2020). Abrupt permafrost thaw is assumed to amplify gradual thaw, since they spread at similar rates in dedicated permafrost models (Turetsky et al., 2020; Armstrong McKay et al., 2022).

90 Collapse of permafrost can be caused by permafrost degradation becoming self-perpetuating due to the heat released by microbial respiration of soil organic carbon, leading to further thaw of permafrost and resulting in a positive feedback loop, which is referred to as the "compost bomb instability" (Luke and Cox, 2011; Khvorostyanov et al., 2008). This process might occur in the Yedoma region or in abruptly dried permafrost soils (Armstrong McKay et al., 2022).

Abrupt dieback of the Amazon is assumed to occur due to reduced moisture recycling and forest-fire-feedbacks triggered by

95 initial tree loss due to either global warming or deforestation, whereby only the former is accounted for in this study (Science Panel for the Amazon, 2021; Nobre et al., 2016).

Our model framework relies on the second version of the Finite amplitude Impulse Response model (FaIR), a 0D reduced complexity climate model developed by Leach et al. (2021), and the estimates for the threshold temperatures, timescales, and impacts of TEs from Armstrong McKay et al. (2022). These estimates are used to build a conceptual carbon tipping elements

100 model (CTEM), which can be coupled to FaIR to include the additional carbon emissions from carbon TEs. With this setup, we generate a "coupled" (CTEM coupled to FaIR) and an "uncoupled" (FaIR only) large-scale model ensemble for all Tier1 shared socioeconomic pathways (SSPs) ~~(O'Neill et al., 2016), propagating~~ except for SSP1-1.9 (O'Neill et al., 2016). Hereby, we propagate the involved uncertainties, up until the year 2500. ~~Even though we give results for all SSPs~~

We exclude SSP1-1.9 from our analysis since it includes a temperature "overshoot" with a pronounced peak of GMST

105 (IPCC, 2021). In case of such a temperature overshoot, tipping elements with internal timescales longer than the period for which GMST exceeds their threshold temperature might remain in their stable baseline state (Ritchie et al., 2021). However, the internal timescales of tipping elements remain highly uncertain, which is why we don't consider the possibility for overshoot of threshold temperatures in this study. To assess the risk of current policies for triggering climate tipping points, we focus our analysis on SSP2-4.5~~and SSP1-2.6. The "middle of the road" scenario SSP2-4.5 is the scenario current policies and actions are~~

110 ~~roughly following, with an estimated warming of~~ . With a median warming of 2.8°C in 2100 produced by FaIR, this scenario is closest to the estimated warming in 2100 resulting from current policies (2.7°C ~~in 2100 (Climate Action Tracker, 2022)~~ ~~. Increased political efforts that would guarantee the timely and complete fulfilment of current climate change mitigation~~ ~~pledges can still limit global warming to 2~~(Climate Action Tracker, 2022), 2.8°C ~~(Meinshausen et al., 2022), consistent with~~ ~~SSP1-2.6. Since SSP1-1.9 might already be politically infeasible to achieve (Jewell and Cherp, 2020), SSP1-2.6 constitutes~~

115 ~~a more realistic "best-case" scenario. To get a sense of how much safer the world would be from crossing climate tipping~~ ~~points when moving away from the current middle of the road towards a more sustainable pathway, it is therefore interesting~~ ~~to compare SSP2-4.5 and SSP1-2.6.~~ (United Nations Environment Programme, 2022), 2.6°C (Meinshausen et al., 2022)).

Our approach is explained in more detail in the next section. In section ~~??~~ 3 we investigate the carbon emissions and ~~their~~ in section 4 the additional warming from carbon TEs, followed by a presentation of the probabilities of triggering TEs in section

120 5. We discuss ~~of~~ our results in section 6 and conclude with section 7.

Category	Proposed Climate Tipping Element (& Tipping Point)		Threshold (°C) Est.	Min	Max	Timescale (years) Est.	Min	Max	Max. Impact (GtC)
Global core tipping elements	PFTP	Boreal Permafrost (collapse)	4.0	3.0	6.0	50	10	300	125 - 250
	GrIS	Greenland Ice Sheet (collapse)	1.5	0.8	3.0	10k	1k	15k	
	WAIS	West Antarctic Ice Sheet (collapse)	1.5	1.0	3.0	2k	500	13k	
	EAIS	East Antarctic Ice Sheet (collapse)	7.5	5.0	10.0	?	10k	?	
	EASB	East Antarctic Subglacial Basin (collapse)	3.0	2.0	6.0	2k	500	10k	
	AWSI	Arctic Winter Sea Ice (collapse)	6.3	4.5	8.7	20	10	100	
	AMAZ	Amazon Rainforest (dieback)	3.5	2.0	6.0	100	50	200	Partial: 30 Total: 75
	AMOC	Atlantic M. O. Circulation (collapse)	4.0	1.4	8.0	50	15	300	
	LABC	Labrador- Irminger Seas SPG Convection (collapse)	1.8	1.1	3.8	10	5	50	
Regional impact tipping elements	PFAT	Boreal Permafrost (abrupt thaw)	1.5	1.0	2.3	200	100	300	Adds 25-75% to gradual thaw: = 5-15 GtC per °C @2100; 12.5-37.5 GtC per °C @2300, up to max. 60-195 GtC
	BARI	Barents Sea Ice (abrupt loss)	1.6	1.5	1.7	25	?	?	
	GLCR	Mountain Glaciers (loss)	2.0	1.5	3.0	200	50	1k	
	REEF	Low-latitude Coral Reefs (die-off)	1.5	1.0	2.0	10	-	-	
	SAHL	Sahel and W. African Monsoon (greening)	2.8	2.0	3.5	50	10	500	
	BORF	Boreal Forest (southern dieback)	4.0	1.4	5.0	100	50	?	52 GtC / -0.18°C
	TUND	Boreal Forest (northern expansion)	4.0	1.5	7.2	100	40	?	-6 GtC / +0.14°C
Threshold-free nonlinear Feedbacks	PFGT	Boreal Permafrost (gradual thaw)	1.5	1.0	2.4	300	100	300<	20 GtC per °C @2100; 50 GtC per °C @2300, up to max 260 GtC

Table 1. Category, threshold, timescale, and impact of the TEs, reproduced from Armstrong McKay et al. (2022). Colours of the second left column represent the Earth system domain of the tipping point (blue = cryosphere, green = biosphere, orange = ocean/atmosphere). All other colours represent confidence, with green = high confidence, yellow = medium confidence and red = low confidence.

2 Data and Methods

2.1 SSP Emission Pathways

We use the CMIP6 GHG and aerosol emissions and effective radiative forcing datasets employed in the Reduced Complexity Model Intercomparison Project (Nicholls et al., 2020). Both datasets contain global average values with an annual timestep throughout the historical period (1750-2014) which shifts to a decadal timestep for the projection period (2015-2500).

The CMIP6 GHG and aerosol emission projections for the five different SSP scenarios follow Gidden et al. (2019). The emission extensions beyond 2100 follow the conventions described in Meinshausen et al. (2020). Historical emissions (1750–2014) of chemically reactive gases (CO, CH_4, NH_3, NO_x, SO_2, non-methane volatile organic compounds) carbonaceous aerosols (black carbon and organic carbon) and CO_2 come from the Community Emissions Data System (Hoesly et al., 2018). Historical biomass burning emissions of CH_4, black carbon, CO, NH_3, NO_X, organic carbon, SO_2 and non-methane volatile organic compounds come from Van Marle et al. (2017). Global historical CO_2 emissions from land-use are taken from the Global Carbon Budget 2016 (Le Quéré et al., 2016). Regional breakdown of land-use CO_2 emissions and N_2O emissions come from the Potsdam Real-time Integrated Model for probabilistic Assessment of emissions Paths for historical emissions version 1.0 (Guetschow et al., 2016). Data gaps in the historical emissions were filled with inverse emissions based on CMIP6 concentrations from the Model for the Assessment of Greenhouse Gas Induced Climate Change (MAGICC) 7.0.0 (Meinshausen et al., 2020).

Effective radiative forcing for CMIP6 follows the data provided by Smith (2020).

2.2 The FaIR Model

To map GHG and aerosol emissions to GMST, including the uncertainty in ECS, we use the ~~second version of the FaIR~~ FaIR v2.0.0 model developed by Leach et al. (2021), which is run with an annual timestep. It consists of six equations, five of which are adopted from Myhre et al. (2013). The sixth equation implements a state-dependency of the carbon cycle, which enables a better representation of the relationship between emissions and atmospheric concentrations for historical observations and projections (Leach et al., 2021). Despite its relative simplicity, FaIR is flexible enough to emulate more complex ESMs from CMIP6. FaIR allows for probabilistic projections of GMST by relying on a parameter ensemble informed by CMIP6 models and constrained with the observed trend and level of global warming. However, this constraint is not strong enough to rule out potentially unrealistic high equilibrium climate sensitivities (ECS) with a 95th percentile of 6.59°C, compared to 5°C reported by Forster et al. (2021). Since we rely on this constrained parameter ensemble to include the uncertainty in ECS in our predictions of GMST, extremely high temperatures towards the end of the model period might be unrealistic.

2.3 Carbon Tipping Elements Model

We introduce the simple, system-dynamics type model CTEM to investigate the carbon emissions that might arise from tipping of AMAZ, PFTP and PFAT and the respective warming caused by them, which, in turn, increases the probabilities of triggering

other TEs. CTEM is able to represent the carbon emissions from AMAZ, PFAT, and PFTP, with threshold temperatures, timescales, and impacts consistent with the estimates from Armstrong McKay et al. (2022) (Table 1). Each TE is represented by a stock of cumulative carbon emissions it adds to the SSP carbon emissions. The cumulative emissions are represented by the following logistic equation:

$$\frac{dS}{dt} = r\left(\frac{T}{P}\right) S\left(1 - \frac{S}{K}\right),\tag{1}$$

with S being cumulative carbon emissions (in GtC), r the maximum growth rate (in yr^{-1}), K the maximum impact (in GtC), P the threshold temperature (in °C), T GMST relative to pre-industrial levels (in °C) and t time (in years). The rate-dependence of all three TEs found by Armstrong McKay et al. (2022) is included by the term T/P, which means higher exceedance of the threshold temperature causes faster change in S.

For AMAZ and PFTP, the impact is independent of GMST once they are triggered (Table 1). Therefore, Eq. 1 can be used to represent them without further modifications being necessary. PFAT, however, is assumed to amplify PFGT, which is a threshold-free feedback. Therefore, the impact of PFAT also depends on GMST, with higher temperatures leading to increased carbon emissions, and different values for this feedback in 2100 and 2300 (Table 1). Hence, for PFAT K from Eq. 1 needs to be calculated as

$$K = \min(F \cdot T, \, K_{\max})\tag{2}$$

with

$$F = \begin{cases} F_{100} & \forall \, t \leq 2100 \\ F_{100} \cdot \frac{2300-t}{200} + F_{300} \cdot \frac{t-2100}{200} & \forall \, 2100 < t < 2300 \\ F_{300} & \forall \, t \geq 2300 \end{cases}\tag{3}$$

Here, K is calculated as the product of the feedback strength F (in $\text{GtC} \, °\text{C}^{-1}$) and GMST (in °C), limited to the maximum impact $K_{\max}$ (in GtC) of PFAT. In Eq. 3, we define F as the feedback strength for the year 2100 (F_{100}) before and in 2100, as the feedback strength for the year 2300 (F_{300}) in and after 2300 and interpolate linearly between these two values between 2100 and 2300.

The resulting set of three differential equations (one for each TE) is solved using a forward difference scheme, similar to the implementation of FaIR (supplement of Leach et al. (2021)). In FaIR, output variables such as T are assumed to be average values between two consecutive timesteps (denoted by a bar over t), while the values for the input variables such as the annual SSP GHG emissions (E_{SSP}) reside at each timestep (no bar over t). To be consistent with this implementation, we define S and the resulting annual carbon emissions from each TE (E_{TE}) also at each timestep (Fig. S1). To calculate S for each timestep (t) with a step size (Δt) of one year, we integrate Eq. 1 which yields:

$$S(t) = \left(e^{-a(\overline{t-1})\Delta t}\left(S^{-1}(t-1) - \frac{b(\overline{t-1})}{a(\overline{t-1})}\right) + \frac{b(\overline{t-1})}{a(\overline{t-1})}\right)^{-1},\tag{4}$$
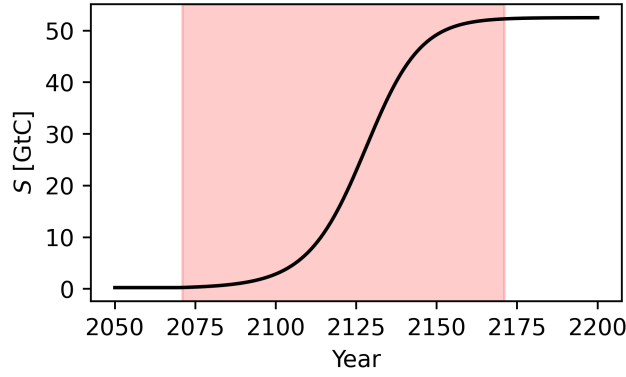
Figure 1. S for the calibration of the mean timescale of AMAZ (under SSP5-8.5). The red shaded area denotes the period over which 99% of the cumulative carbon emissions occur.

180 with the auxiliary variables a and b being calculated as

$$a(\overline{t-1}) = r\frac{T(\overline{t-1})}{P}$$
$$b(\overline{t-1}) = \frac{rT(\overline{t-1})}{PK}.$$

For PFTP and AMAZ Eq. 4 can be used directly to calculate S, but for PFAT K needs to be calculated using Eq. 2 with $T = T(\overline{t-1})$ and is therefore also time-dependent (for the full derivation please see ~~Sect.S1~~ Section S2). Irreversibility of

185 carbon emissions from all three TEs is implemented by setting negative changes of S to zero.

CTEM needs to be calibrated to match the estimated behaviour summarised in Table 1. While values for F_{100}, F_{300}, K, $K_{\max}$, and P can be used in CTEM directly, r and the initial stock (S_0) need to be calibrated or defined for the model to match the proposed tipping timescales (H). For this purpose, we define the H as the period over which 99% of the cumulative emissions occur. While H and the corresponding value of r are calibrated for the whole range of H given in Table 1 for PFTP

190 and AMAZ, PFAT is implemented slightly different since K depends on T (Eq. 2). For PFAT, H is included implicitly in the feedback parameters F_{100} and F_{300}, with high values corresponding to short H and vice versa. Therefore, we keep H and the corresponding r fixed at their mean value for PFAT, with varying values for the feedback parameters. In the calibrated version of CTEM, the evolution of S follows the characteristic S-shape of logistic equations (Fig. 1). Further information on the calibration of CTEM is given in ~~Sect. S2.~~ Section S3. A test of the calibration yields that the timescales produced by

195 CTEM are generally matching the expected behaviour for AMAZ and PFTP (Fig. S3), but not for PFAT (Fig. S4). For PFAT we find that the carbon emissions are generally too low in 2100, however, this emission deficit is removed until 2300, where emissions of PFAT match the estimates. We regard this deviation to be acceptable, given the simplicity of our model approach (see ~~Sect.S3~~ Section S4 for further information).

2.3.1 Coupling to FaIR

CTEM is coupled to FaIR every timestep by adding E_{TE} to E_{SSP}. For each TE, we calculate E_{TE} from S as

$$E_{\mathrm{TE}}(t) = S(t) - S(t-1).$$

The total carbon emissions E_{TE} are split up into CO_2 and CH_4 emissions for all three TEs. For PFAT, we assume that 20% of the carbon is emitted as CH_4, following Turetsky et al. (2020), while no CH_4 emissions are expected from AMAZ (Armstrong McKay et al., 2022). Quantifying the fraction of CH_4 emissions arising from PFTP is challenging due to the lack of previous model studies and limited process understanding. We rely on the 2D model study conducted by Schneider von Deimling et al. (2015), who report 40% of additional warming due to CH_4 emissions from the Yedoma deposits, which can be associated with PFTP. Since this amplification is within the uncertainty range of additional warming caused by CH_4 emissions from gradual permafrost thaw of $35-48\%$ for which 2.3% of the carbon is emitted as methane (Schuur et al., 2015), we assume that this fraction of CH_4 emissions also holds for PFTP. The annual CH_4 and CO_2 emissions of all three TEs are then added to $E_{\mathrm{SSP}}(t)$ of the respective SSP and the sum is used to run the next timestep of FaIR, calculating $T(\bar{t})$ which is then used to force CTEM and so on.

To avoid double counting of carbon emissions, carbon emissions from the carbon TEs modelled by CTEM must not be included in FaIR. We can rule this possibility out, since carbon emissions from carbon TEs are neither accounted for by the CMIP6 models used to parameterize FaIR, nor of major importance for the observed warming signal used to constrain the parameter ensemble (See Section S6 for further explanation and references).

2.4 Generation of Model Ensembles

We construct a coupled (FaIR coupled to CTEM) and an uncoupled (FaIR only) 5000 members model ensemble for ~~all five Tier1 SSPs~~SSP1-2.6, SSP2-4.5, SSP3-7.0 and SSP5-8.5. Hereby, we follow a Monte Carlo scheme (Metropolis et al., 1953) to propagate the uncertainties within FaIR and CTEM.

For the parameterization of FaIR, we randomly select 5000 members of its constrained parameter ensemble. We use the same parameter sample for FaIR in both the coupled and the uncoupled ensemble to make sure that changes in the climate response only arise from carbon emissions of the carbon TEs.

For the parameterization of CTEM and the calculation of triggering probabilities, we construct probability distributions of the respective parameters based on the estimates given in Table 1. From those probability distributions, we sample parameter values, employing Latin hypercube sampling (McKay et al., 1979).

To calculate the probability of triggering, we sample the uncertainty range of P for all TEs, again using the same parameter sample for both ensembles. For the sampling process of P, we infer probability distributions from the estimates in Table 1, deciding that the minimum estimate, the best estimate, and the maximum estimate should correspond to the 5th, the 50th and the 95th percentile of the respective probability distribution. To determine the probability distributions which best fits those percentiles, we use the "rriskDistributions" package (Belgorodski et al., 2017), which chooses out of 17 continuous probability
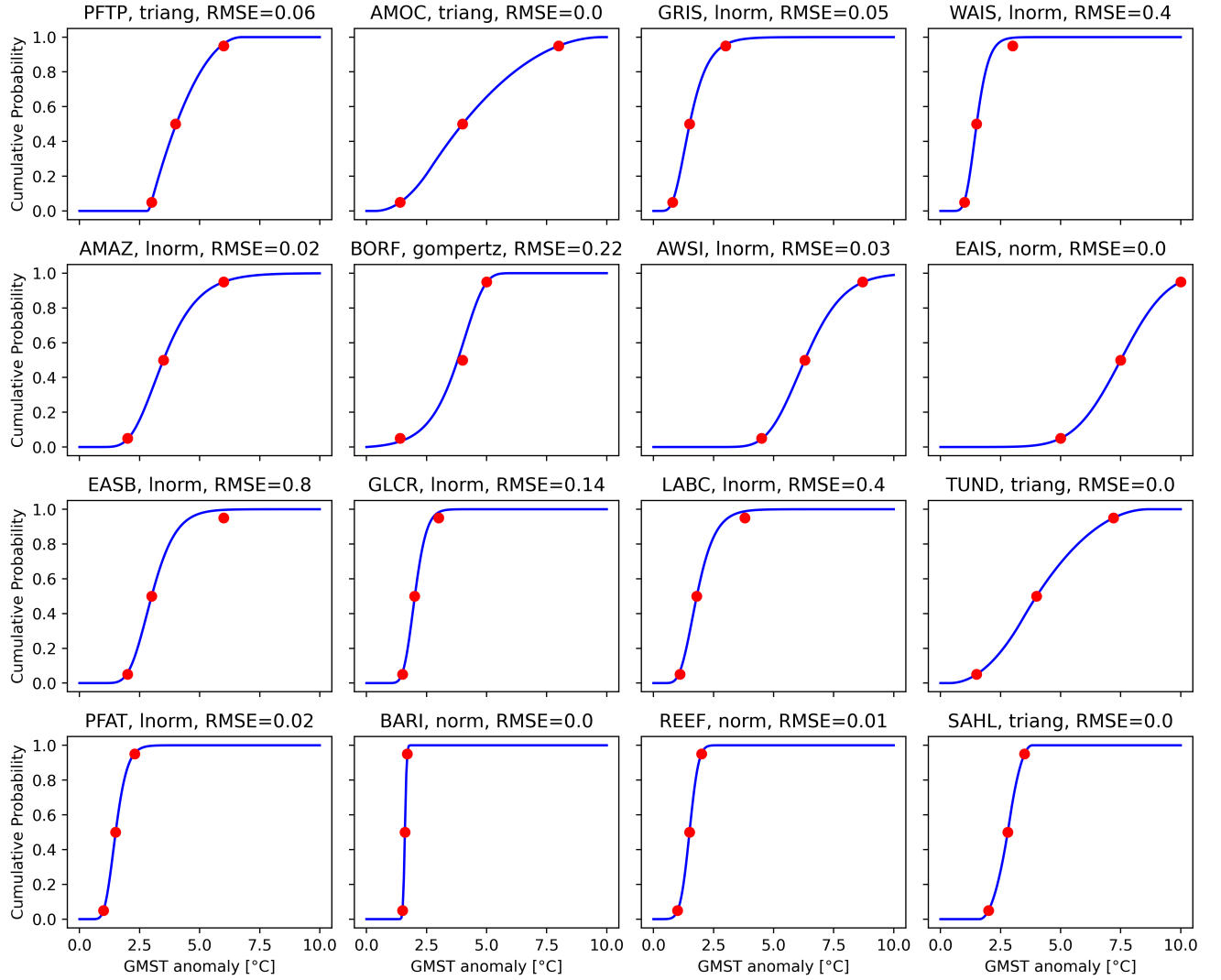
Figure 2. Cumulative distribution functions of P for all TEs, together with the RMSE between the given percentiles (red dots) and the actual percentiles of the respective distribution. The title states TE, distribution type and RMSE in °C.

distributions, minimizing the absolute difference between the given and the actual percentiles. We derive eight log-normal, four triangular, three normal and one Gompertz distribution (Fig. 2). While some distributions of P agree perfectly with the given percentiles (AMOC, EAIS, TUND, BARI, SAHL), others deviate substantially with RMSEs higher than 0.2°C (WAIS, BORF, EASB, LABC). In the case of WAIS, EASB, and LABC this deviation is mainly caused by too low values at the 95th percentile, which is reached at 2.3°C rather than 3°C for WAIS, 4.6°C rather than 6°C for EASB, and 3.1°C rather than 3.8°C for LABC. In the case of BORF, the relatively high RMSE is caused by a too high value at the 5th percentile (1.7°C rather than 1.4°C) and a too low value at the 50th percentile (3.8°C rather than 4°C), while the 95th percentile agrees well with the expected value (less than 0.02°C deviation). Even though the deviations between the given and the actual percentiles of those four TEs are significant, we regard them to be acceptable, given that they cannot be reduced with our methodology, meaning that other probability distributions would be needed to achieve this. However, it must be kept in mind that high probabilities of tipping might be reached at too low values of GMST for WAIS, EASB and LABC due to their imperfect probability distributions of P.

We now turn to the parameterization of CTEM. For the distribution of H for PFTP and AMAZ, we derive one log-normal distribution each, following the same approach as for the generation of probability distributions of P (Fig. S5). The impacts K of PFTP and AMAZ and the maximum impact $K_{\max}$ of PFAT are sampled from continuous uniform distributions, with the same probability for all values within the given ranges from Table 1 (Fig. S6). We regard this reasonable since Armstrong McKay et al. (2022) only give maximum and minimum values for those variables, and we do not have any additional information about their distribution. The feedback strengths F_{100} and F_{300} of PFAT are also sampled from continuous uniform distributions, with the same probability for all values within the given ranges from Table 1 (Fig. S7). Here, the same argument holds as for the selection of the distributions of K and $K_{\max}$.

We assume that all parameters within the parameter set of CTEM are uncorrelated, except for F_{100} and F_{300}, which are correlated with a correlation coefficient of 1. The decision about the correlation of the parameters represents our understanding that there are no correlations, or at least no clear evidence for them, between the threshold temperatures, the timescales, or the impacts of AMAZ, PFAT and PFTP. The correlation between F_{100} and F_{300} is established since H of PFAT is included in those parameters, and we assume that H is constant over time, e.g., a low feedback in 2100 associated with a high H also means low feedback in 2300 due to the same high H the emissions occur over.

2.5 Calculation of Tipping Probabilities

To calculate the probabilities of triggering any of the 16 TEs discussed in this study, we sample one value of P from the respective distribution (Fig. 2) for each TE and each ensemble member. If T of that ensemble member exceeds P, the TE is counted as triggered. In this manner, we derive the share of ensemble members in which a TE is triggered for each TE at all times. As all TEs discussed here are by definition irreversible on the considered timescale, the share of triggered TEs cannot decrease with time, even if T would decrease. The share of ensemble members with triggered TEs is then used to further investigate the probabilities of triggering, e.g., by calculating the timing of the exceedance of certain share percentages.

2.6 Robustness of the Results

265 To examine whether an ensemble of size 5000 is sufficiently large to approximate the distributions of the output variables with our Monte Carlo approach, we create 20 coupled ensembles with 5000 members and run under SSP5-8.5, sampling uncertainties within FaIR and CTEM. As carbon emissions from CTEM are used to calculate T, which is also the final output variable of FaIR, it includes uncertainties from all parameters and is hence expected to vary most between different ensembles. Therefore, we inspect the deviation of T between the 20 ensembles. While the 5th percentile and the mean of T are nearly

270 equal for all ensembles, with standard deviations below 0.06°C at all times, the 95th percentile deviates slightly between the ensembles, with a standard deviation of up to 0.24°C (Fig. S8). Given the range of T between the 5th and the 95th percentile of ~ 11°C, we regard those deviations to be sufficiently small.

3 ~~Impacts of~~ Carbon Emissions from Carbon Tipping Elements

~~We now turn to the presentation of our results. For the description of probabilities we use the calibrated language of the IPCC:~~
275 ~~virtually certain: 99 − 100%, extremely likely: 95 − 100%, very likely: 90 − 100%, likely: 66 − 100%, more likely than not:~~
~~>50 − 100%, about as likely as not: 33 − 66%, unlikely: 0 − 33%, very unlikely: 0 − 10%, and extremely unlikely: 0 − 5%~~
~~(Chen et al., 2021).~~

3.1 ~~Additional Carbon Emissions~~

The carbon emissions from carbon TEs increase from ~~SSP1-1.9~~ SSP1-2.6 to SSP5-8.5 (~~Table 2, Fig. S9~~ Fig. 3, Table 2). While
280 zero carbon emissions from carbon TEs remain possible under ~~SSP1-1.9 and~~ SSP1-2.6, high carbon emissions become much more likely under SSP2-4.5, with the maximum emissions being nearly as high as under SSP5-8.5 ~~(Table 2)~~. This is a direct consequence of the probabilities of triggering carbon TEs. Under SSP1-2.6 ~~only~~, triggering of PFAT ~~becomes likely in the~~ ~~coupled ensemble (82%)~~ occurs for 79% of the ensemble members, while triggering of AMAZ and PFTP ~~remains unlikely~~ ~~(only happens for~~ 13% and 5% respectively~~)~~. Under SSP2-4.5, triggering probabilities are increased substantially, to 98% for
285 PFAT, ~~55~~53% for AMAZ and ~~38~~37% for PFTP. This means that maximum carbon emissions with all three carbon TEs triggered become more likely under SSP2-4.5 compared to SSP1-2.6.

Even though the highest carbon emissions from carbon TEs ~~are emitted~~ occur under SSP3-7.0 and SSP5-8.5, they remain small compared to anthropogenic carbon emissions (Fig. 3). The 95th percentile of cumulative carbon emissions from carbon TEs only reaches 14% of the cumulative anthropogenic carbon emissions in 2500 under SSP3-7.0, and ~~9~~10% under SSP5-8.5.
290 The relative contribution of carbon emissions from carbon TEs to the total carbon emissions increases towards lower emission scenarios. Under SSP2-4.5 the 95th percentile of cumulative carbon emissions from carbon TEs reaches 35% of the cumulative anthropogenic carbon emissions in 2500, and 40% under SSP1-2.6 ~~and 84% under SSP1-1.9~~.

Hence, SSP2-4.5 is special in the sense that maximum carbon emissions from carbon TEs are already possible and are large relative to the anthropogenic emissions.
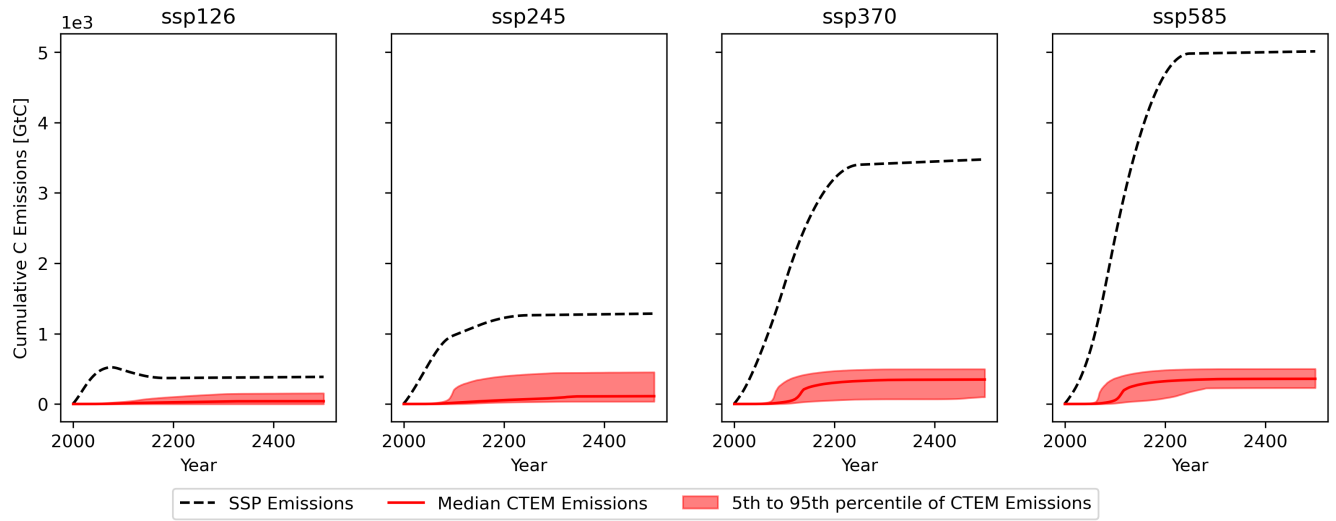
Figure 3. ~~Carbon emissions and cumulative~~ Cumulative carbon emissions from ~~the Tier1~~ all SSP scenarios and the carbon TEs (modelled by CTEM) between 2000 and 2500.

		2050	2100	2200	2300	2400	2500
~~SSP1-1.9~~							
~~CO₂~~	~~GtC~~	~~1 (0-5)~~	~~5 (0-19)~~	~~11 (0-36)~~	~~16 (0-58)~~	~~18 (0-63)~~	~~18 (0-66)~~
~~CH₄~~	~~GtCH₄~~	~~0.3 (0-1.5)~~	~~1.8 (0-5.6)~~	~~3.5 (0-10.2)~~	~~5.3 (0-16.7)~~	~~5.9 (0-17.8)~~	~~6 (0-18.3)~~
~~dT~~	~~°C~~	~~0.01 (0-0.07)~~	~~0.04 (0-0.17)~~	~~0.03 (0-0.2)~~	~~0.05 (0-0.29)~~	~~0.03 (0-0.23)~~	~~0.03 (0-0.22)~~
SSP1-2.6							
CO_2	[GtC]	1 (0-5)	8 (~~0-29~~0-28)	20 (~~0-85~~0-84)	30 (~~0-121~~0-120)	~~33 (0-136~~32 (0-135)	~~33~~32 (0-152)
CH_4	[GtCH₄]	0.3 (0-1.~~6~~5)	~~2.6~~2.5 (0-7.5)	~~6.4~~6.3 (0-15.9)	~~9.8~~9.6 (0-25.~~3~~2)	10.5 (~~0-27~~10.4 (0-26.9)	~~10.7~~10.5 (0-27.~~8~~7)
dT	[°C]	0.01 (0-0.07)	~~0.07~~0.06 (0-0.24)	0.08 (0-0.34)	0.1 (0-0.~~49~~48)	0.06 (0-0.47)	0.06 (0-0.~~53~~54)
SSP2-4.5							
CO_2	[GtC]	1 (~~0-6~~0-5)	~~16 (2-155~~15 (1-148)	~~67 (19-324~~64 (19-323)	~~102~~99 (28-359)	~~108 (30-365~~105 (29-365)	~~112 (30-369~~109 (39-368)
CH_4	[GtCH₄]	0.3 (0-1.~~8~~7)	~~4.7 (0.4-13.6~~4.6 (0.3-13.5)	~~15.6~~15.4 (6.3-~~33~~32.9)	~~21.9 (9.2~~21.8 (9.1-43.3)	~~22.8 (9.6-44.7~~22.6 (9.5-44.6)	~~23.1 (9.7-45.3~~22.9 (9.5-45.1)
dT	[°C]	0.01 (0-0.~~08~~07)	0.13 (~~0.02-0.61~~0.01-0.59)	0.2 (0.06-0.85)	~~0.22~~0.21 (0.06-0.91)	0.16 (0.03-0.89)	~~0.16~~0.15 (0.03-0.91)
SSP3-7.0							
CO_2	[GtC]	1 (0-6)	~~34 (6-245~~33 (5-242)	285 (~~91-381~~89-381)	318 (143-403~~317 (137-403)	322 (~~154-406~~147-406)	~~324 (160-407~~323 (152-407)
CH_4	[GtCH₄]	~~0.4~~0.3 (0-1.~~9~~8)	8.1 (~~1.5~~1.4-20)	29.3 (17-47.5)	~~35.2 (22.9-53.9~~35.1 (22.8-53.7)	35.6 (~~23.4~~23.3-53.9)	35.9 (~~23.6~~23.4-54)
dT	[°C]	0.01 (0-0.~~08~~07)	0.25 (~~0.05-0.94~~0.04-0.93)	0.39 (0.15-0.~~81~~0.82)	0.31 (~~0.13~~0.12-0.66)	0.27 (~~0.10~~0.09-0.63)	0.26 (0.09-0.63)
SSP5-8.5							
CO_2	[GtC]	~~2~~1 (0-8)	~~78 (13-283~~76 (13-282)	304 (~~138-389~~136-389)	328 (~~235-408~~233-408)	330 (~~244-410~~243-410)	331 (246-411)
CH_4	[GtCH₄]	~~0.5~~0.4 (0-2.~~3~~2)	~~12.4 (3.3~~12.2 (3.1-26.2)	32 (~~20.6~~20.5-50.5)	37.1 (24.1-54.3)	37.4 (24.3-54.6)	37.7 (24.3-54.7)
dT	[°C]	0.02 (0-0.~~1~~09)	0.4 (0.09-1.11)	0.31 (0.13-0.64)	0.23 (0.1-0.52)	0.19 (0.08-0.47)	0.18 (0.08-0.47)

Table 2. Median and ~~very likely range (~~ 5th – 95th percentile ~~)~~ range of cumulative CO_2 and CH_4 emissions from the carbon TEs and the GMST increase (dT) caused by them. All quantities are calculated individually for each ensemble member as the increase caused by carbon TEs compared to the respective uncoupled ensemble member.
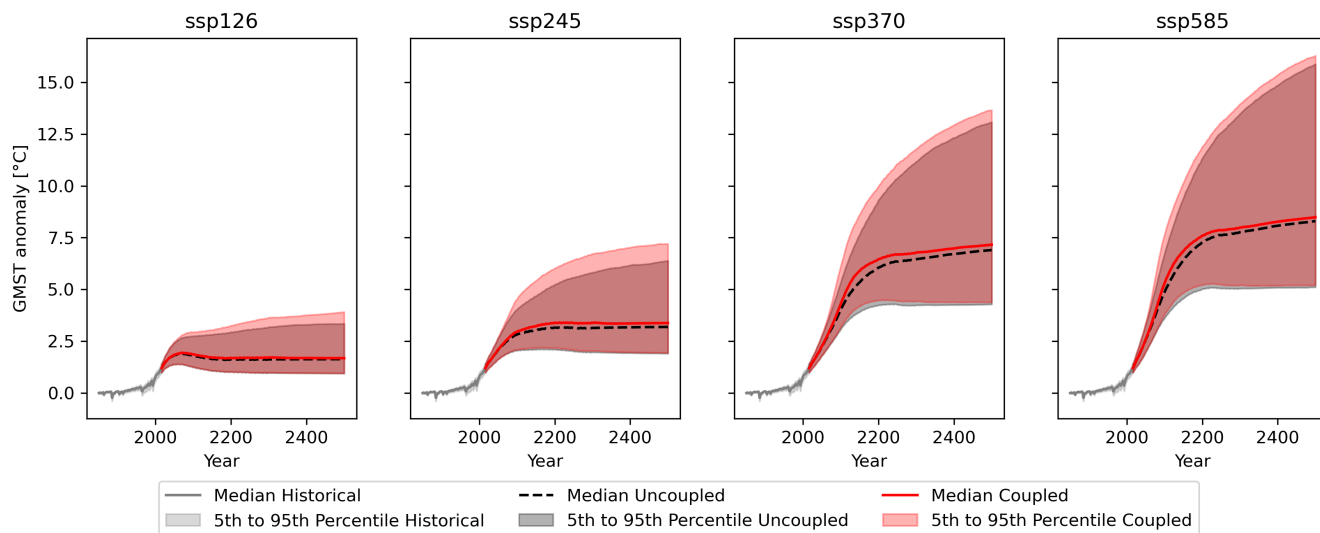
Figure 4. GMST relative to the 1850-1900 period of the coupled and the uncoupled ensemble~~for the Tier1 SSPs~~, together with the historical evolution.

3.1 ~~Increase of Global Warming~~

4 Increase of Global Warming Caused by Carbon Tipping Elements

The carbon emissions from carbon TEs cause an increase in global warming (Fig. 4). Under ~~the low emission scenarios SSP1-1.9 and~~ SSP1-2.6, high temperature increases from carbon TEs are possible but ~~less~~ not common, with the temperature distributions skewed towards higher values. No ~~temperature increase~~ additional warming from carbon TEs remains possible under ~~those scenarios, as it is still within the very likely range~~ this scenario, with the 5th percentile being zero at all times (Table 2). ~~The median temperature increase from carbon TEs also remains relatively small, reaching maximum values of 0.05°C and 0.1°C in 2300 under SSP1-1.9 and SSP1-2.6 respectively. However, the upper end of the very likely range of the temperature increase from carbon TEs reaches maxima of 0.29°C in 2300 under SSP1-1.9 and 0.53°C in 2500 under SSP1-2.6, which would mean a 26% and 32% temperature increase respectively compared to the median of the uncoupled ensemble.~~

~~For~~ Under SSP2-4.5, high impacts from carbon TEs ~~remain an exception (Fig. 4), however, compared to the low emission scenarios high temperature increases~~ become more common ~~, as reflected~~ compared to SSP1-2.6. This is indicated by the median temperature increase, which reaches its maximum of 0.22°C in 2300 ~~(Table 2). Even though the warming caused by anthropogenic carbon emissions has increased~~ under SSP2-4.5, ~~the additional warming caused by carbon TEs can still cause high relative temperature increases. In 2500 the upper end of the very likely range of additional warming from carbon TEs reaches 0.91~~compared to only 0.08°C being reached in the same year under SSP1-2.6 (Table 2)~~, which constitutes a temperature increase of 29% compared to the median of the uncoupled ensemble.~~

. Additional warming from carbon TEs becomes the default case under the high emission scenarios SSP3-7.0 and SSP5-8.5. ~~However, this additional warming becomes small compared to the warming from anthropogenic carbon emissions. In 2500~~ The 5th percentile of the temperature increase is well above zero after 2100 for both scenarios and the median reaches 0.39°C and 0.4°C in 2300 and 2200 under SSP3-7.0 and SSP5-8.~~5 the upper end of the very likely range of additional~~.5 respectively (Table 2).

High additional warming from carbon TEs mostly occurs for ensemble members with a high climate sensitivity. This is indicated by the 95th percentile of the temperature distribution increasing more than all other percentiles if the warming from carbon TEs ~~reaches 0.47°C (Table 2), which only constitutes a temperature increase of 6% compared to the median of the uncoupled ensemble.~~ is included (Fig. 4). This effect is especially pronounced under SSP1-2.6 and SSP2-4.5.

It is interesting to see that the highest long-term temperature increase from carbon TEs becomes possible under SSP2-4.5, with the 95th percentile reaching 0.91°C in 2500, and not under scenarios with higher anthropogenic emissions (Table 2). This is in contradiction to the cumulative CO_2 and CH_4 emissions from carbon TEs, which are higher under high emission scenarios than under SSP2-4.5~~(Table 2)~~. The reason for this behaviour is the implementation of the forcing relationship translating atmospheric CO_2 and CH_4 concentrations to radiative forcing developed by Etminan et al. (2016) and used in FaIR. It is approximated by a logarithmic and a square-root term for CO_2 and by a square-root term for CH_4, meaning that the effect of additional atmospheric concentrations of both GHGs on GMST is decreasing for higher atmospheric concentration levels. ~~This means that~~ Therefore, the amount of carbon emissions from carbon TEs relative to the anthropogenic emissions is decisive to determine the additional warming from carbon TEs.

Nevertheless, it must be noted that the highest short-term temperature increase from carbon TEs becomes possible under the high emissions scenarios SSP3-7.0 and SSP5-8.5, with the upper end of the very likely range reaching 0.94°C and 1.11°C in 2100 under SSP3-70 and SSP5-8.5 respectively. This can be linked to high ~~transient~~ CH_4 emissions from fast PFAT degradation due to rapidly increasing temperatures, which leads to peaks in the atmospheric CH_4 concentration anomaly around 2100 (Fig. ~~S10~~S9).

The temperature increase from carbon TEs occurs earlier under high emission scenarios (Table 2), which can be explained by threshold temperatures of the carbon TEs being crossed earlier under those scenarios, as the general temperature increase is faster (Fig. 4). Interestingly, the median temperature increase from carbon TEs is declining towards the end of the model period under all SSPs (Table 2). This can be linked to the decreasing atmospheric methane concentrations (Fig. ~~S10~~S9).

When comparing the different SSPs, it becomes evident that high temperature increases from carbon TEs are possible but rare under low emission scenarios, and become more frequent but less strong compared to the anthropogenic warming under high emission scenarios (Table 2 and Fig. 4). This means that if anthropogenic carbon emissions can be limited to levels comparable to SSP1-2.6, there remains a risk that the warming might be substantially increased by triggering carbon TEs. On the other hand, if anthropogenic emissions keep increasing like under SSP5-8.5 warming will almost certainly be amplified by carbon TEs, however, this additional warming will remain small compared to the anthropogenic warming. On average, the additional warming from carbon TEs is low compared to the anthropogenic warming and the risk for high temperature

5   Probabilities of Triggering Climate Tipping Elements

We now turn to the probabilities of triggering any of the 16 TEs proposed by Armstrong McKay et al. (2022) (Table 1), and
350   how those probabilities are increased by the additional warming from carbon TEs. To compare those probabilities among the SSPs, we focus on the crossing of 50% probability, where triggering becomes more likely than not.

The effect of carbon TEs on the probabilities of triggering TEs under the different SSP scenarios is clearly visible, with triggering getting more likely earlier if carbon emissions from carbon TEs are included (Fig. 5). On average, TEs become more likely than not to be triggered ~~9.3~~ 6.6 years earlier if carbon emissions from carbon TEs are included. This effect becomes more
355   pronounced towards the end of the prediction period, since GMST is generally increasing slower at that time, which means it takes longer for the uncoupled ensemble to reach the same temperatures as the coupled ensemble (Fig. 4). Especially TEs within the cryosphere ~~can~~ will become more likely than not to be triggered decades earlier, if carbon emissions from carbon TEs are included. EAIS and AWSI cross the 50% probability of triggering 25 years and 19 years earlier respectively under SSP5-8.5, AWSI crosses it ~~47~~ 50 years earlier under SSP3-7.0, and EASB crosses it ~~26~~ 30 years earlier under SSP2-4.5 ~~, and~~
360   ~~GLCR crosses it 348 years earlier under SSP1-2.6~~ (Fig. 5). As we do not consider any interactions between the TEs apart from the increase in GMST from carbon TEs, the fact that crossing of a certain probability level is ~~reached disproportionately~~ achieved significantly earlier for some TEs if carbon emissions from carbon TEs are included is solely caused by a favourable combination of the threshold temperature distribution and the maximum temperatures reached under the respective SSP and should therefore not be over interpreted.
365   Even though additional probability of triggering caused by carbon emissions from carbon TEs clearly exists, it remains small compared to the probability of triggering caused by anthropogenic carbon emissions. Only ~~two~~ three TEs become more likely than not to be triggered in addition to the uncoupled ensemble due to the inclusion of carbon TEs in the sum over all SSPs (Fig. 5). Carbon TEs do not cause high enough temperature increases to induce rapid triggering of multiple TEs following the tipping of the carbon TEs. Partly, this might be due to the fact that PFTP, which causes the highest carbon emissions of all

	Probability of Triggering [%]	Probability Increase from Carbon TEs [pp]
~~SSP1-1.9 28 1.1~~ SSP1-2.6	~~38~~ 37	~~2.3~~ 2.2
SSP2-4.5	~~65~~ 64	3.3
SSP3-7.0	~~92~~ 91	1.0
SSP5-8.5	95	~~0.4~~ 0.5

Table 3. Probability of triggering averaged over all TEs in 2500 and its increase due to additional warming caused by carbon emissions from carbon TEs in percent points (pp).
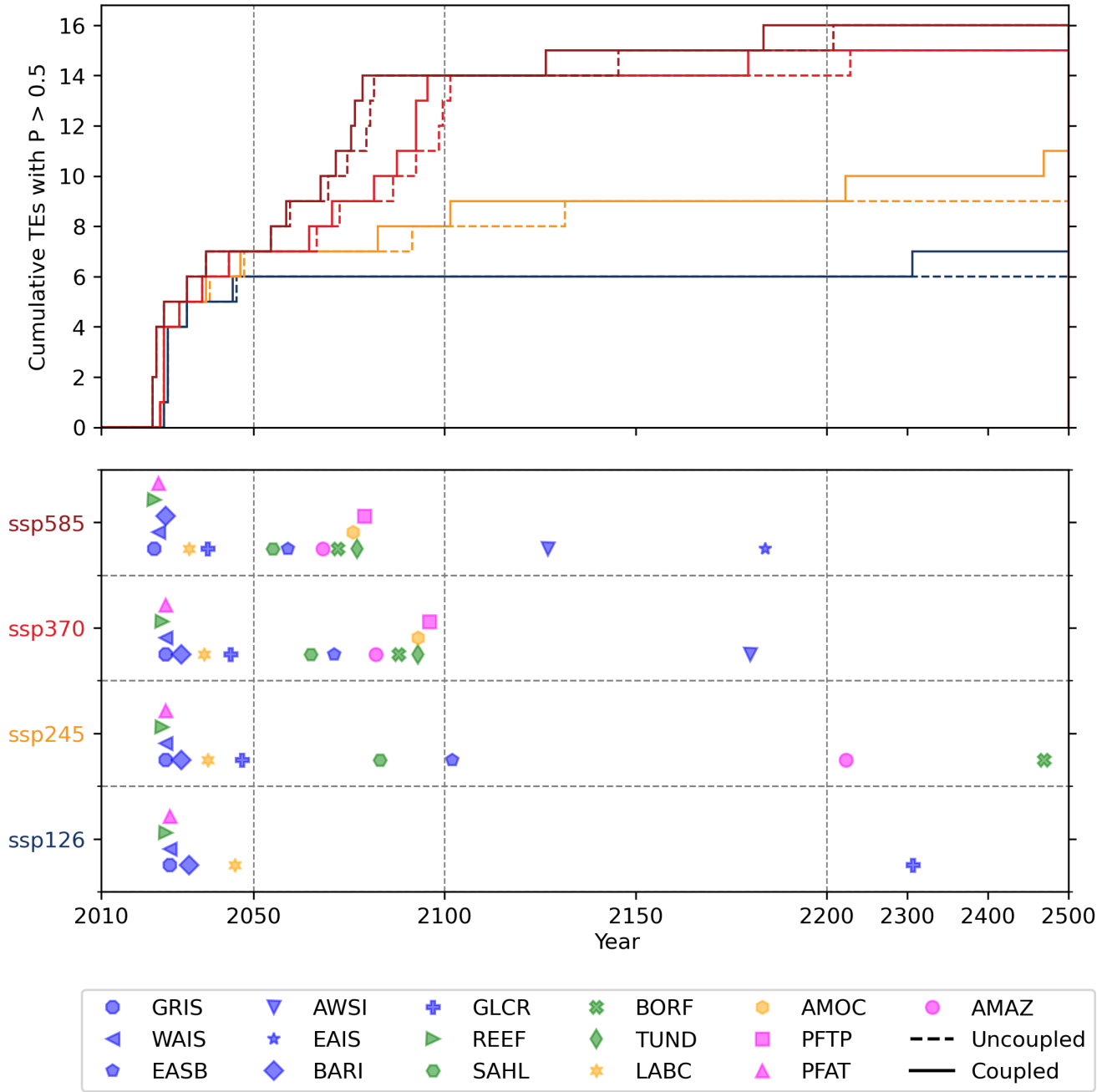
Figure 5. Cumulative number of TEs with a more than 50% probability (P) of getting triggered for the Tier1 SSP scenarios from the coupled and the uncoupled ensemble (upper row) and symbols of the triggered TEs corresponding to the increase of cumulative TEs in the coupled ensemble (lower row). Carbon TEs are marked with pink symbols, whereas the other TEs are marked in the colours suggested by Armstrong McKay et al. (2022), with blue for cryosphere, green for biosphere and orange for atmospheric or oceanic circulations.

	AMAZ	AMOC	AWSI	BARI	BORF	EAIS	EASB	GLCR	GRIS	LABC	PFAT	PFTP	REEF	SAHL	TUND	WAIS
0.5	2068	2076	2127	2027	2072	2184	2059	2038	2024	2033	2025	2079	2024	2055	2077	2025
0.5	2070	2080	2146	2027	2075	2209	2060	2038	2024	2033	2025	2082	2024	2055	2081	2025
0.95	2142			2039	2116		2098	2060	2062	2067	2049	2152	2043	2080	2404	2049
0.95	2161			2040	2129		2105	2061	2063	2069	2049	2167	2043	2082		2049

Figure 6. Probabilities of triggering the TEs by 2500 under SSP5-8.5. Additional probabilities from the carbon TEs are marked in purple. The table underneath states the years in which the 50% and 95% probability is crossed, with purple including carbon emissions from carbon TEs and black not.

370 carbon TEs, is one of the last TEs to be triggered and hence has little potential to cause earlier triggering of other TEs (Fig. 5). Moreover, even if all carbon TEs are extremely likely to be triggered, they only cause an increase of GMST of up to 0.4°C in the median under SSP5-8.5, which is too small to achieve crossing of multiple TE threshold temperatures (Table 2).

For the exceedance of the 50% probability of triggering, we observe clustering of the TEs, which has the potential to occur earlier if carbon emissions from carbon TEs are included. The first cluster consisting of ~~four~~ five TEs (GRIS, WAIS, REEF,
375 ~~and PFAT) become~~ PFAT, and BARI) becomes more likely than not to be triggered by ~~2026~~2033, regardless of the emission scenario or whether carbon emissions from carbon TEs are included or not (Fig. 5). ~~Three additional TEs forming the second cluster (BARI,~~ LABC and GLCR ~~)~~ also exceed the 50% probability of being triggered before 2050 under SSP2-4.5, SSP3-7.0 and SSP5-8.5. ~~This is much delayed under SSP1-2.6, and can be partly avoided under SSP1-1.9 since only BARI becomes more likely to be triggered than not in 2031. The third~~ A second cluster of seven TEs (SAHL, EASB, AMAZ, BORF, AMOC,
380 TUND, and PFTP) crosses the 50% probability of triggering between 2050 and 2100 under SSP5-8.5 and SSP3-7.0. This can
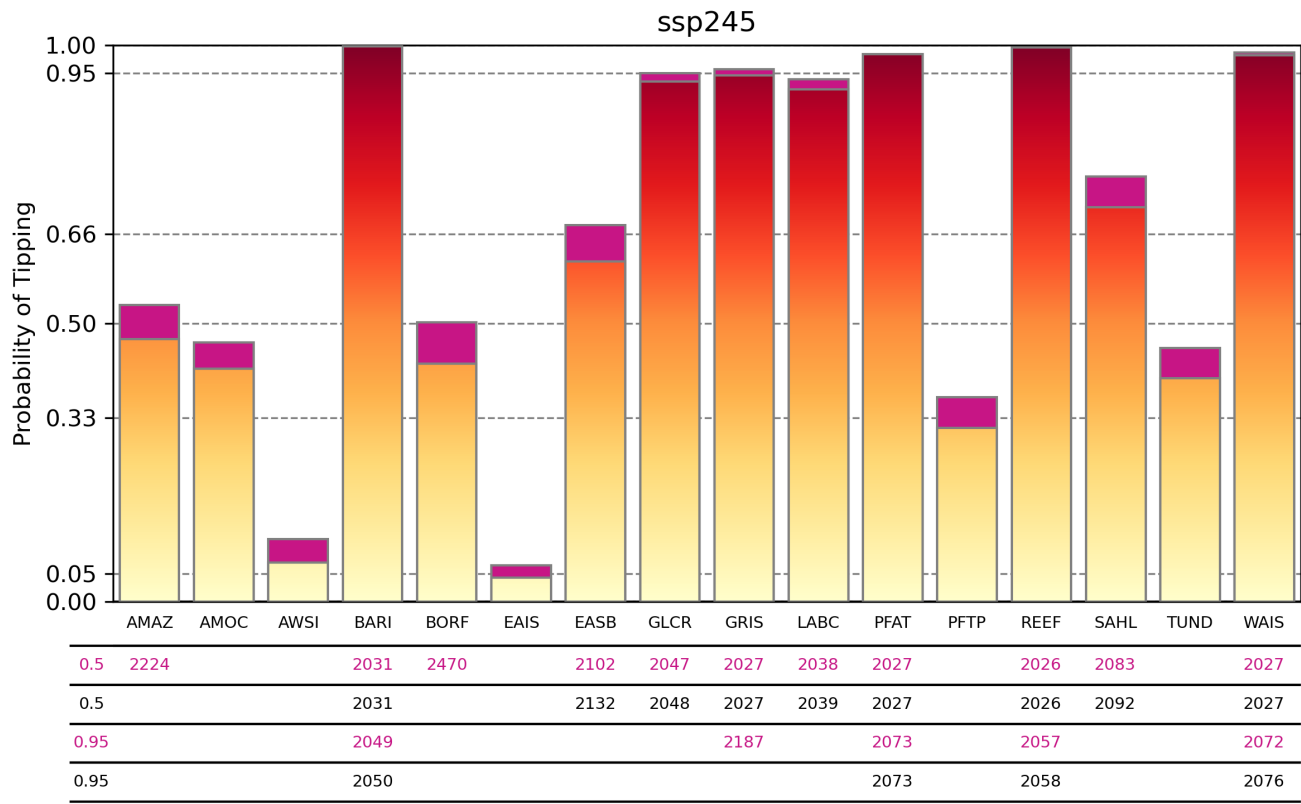
Figure 7. Probabilities of triggering the TEs by 2500 under SSP2-4.5. Additional probabilities from the carbon TEs are marked in purple. The table underneath states the years in which the 50% and the 95% probability are crossed, with purple including carbon emissions from carbon TEs and black not.

	AMAZ	AMOC	AWSI	BARI	BORF	EAIS	EASB	GLCR	GRIS	LABC	PFAT	PFTP	REEF	SAHL	TUND	WAIS
0.5	2224			2031	2470		2102	2047	2027	2038	2027		2026	2083		2027
0.5				2031			2132	2048	2027	2039	2027		2026	2092		2027
0.95				2049					2187		2073		2057			2072
0.95				2050							2073		2058			2076

be partly avoided under SSP2-4.5 with only SAHL and EASB and if carbon emissions from carbon TEs are included also AMAZ and BORF becoming more likely than not to be triggered until 2500. Under ~~SSP1-1.9 and~~ SSP1-2.6, none of the TEs from the third cluster ~~becomes~~ become more likely to be triggered than not, independent of carbon emissions from the carbon TEs. The two remaining TEs AWSI and EAIS do also exceed the 50% probability of being triggered under SSP5-8.5 until 2300, while this is only the case for AWSI under SSP3-7.0. Hence, all 16 TEs are more likely than not to be triggered by 2500 under SSP5-8.5, 15 under SSP3-70, eleven (nine) under SSP2-4.5, ~~seven~~ and seven (six) under SSP1-2.6 ~~and five under SSP1-1.9~~ including (not including) the carbon emissions from carbon TEs.

While the above inspection of the 50% probability level is especially valuable to understand the timing of triggering TEs, a more thorough analysis of the triggering probabilities is needed to fully understand how the risk of triggering TEs changes for the different SSPs. We turn to this part now. To compare the general risk of triggering TEs and how it is amplified by
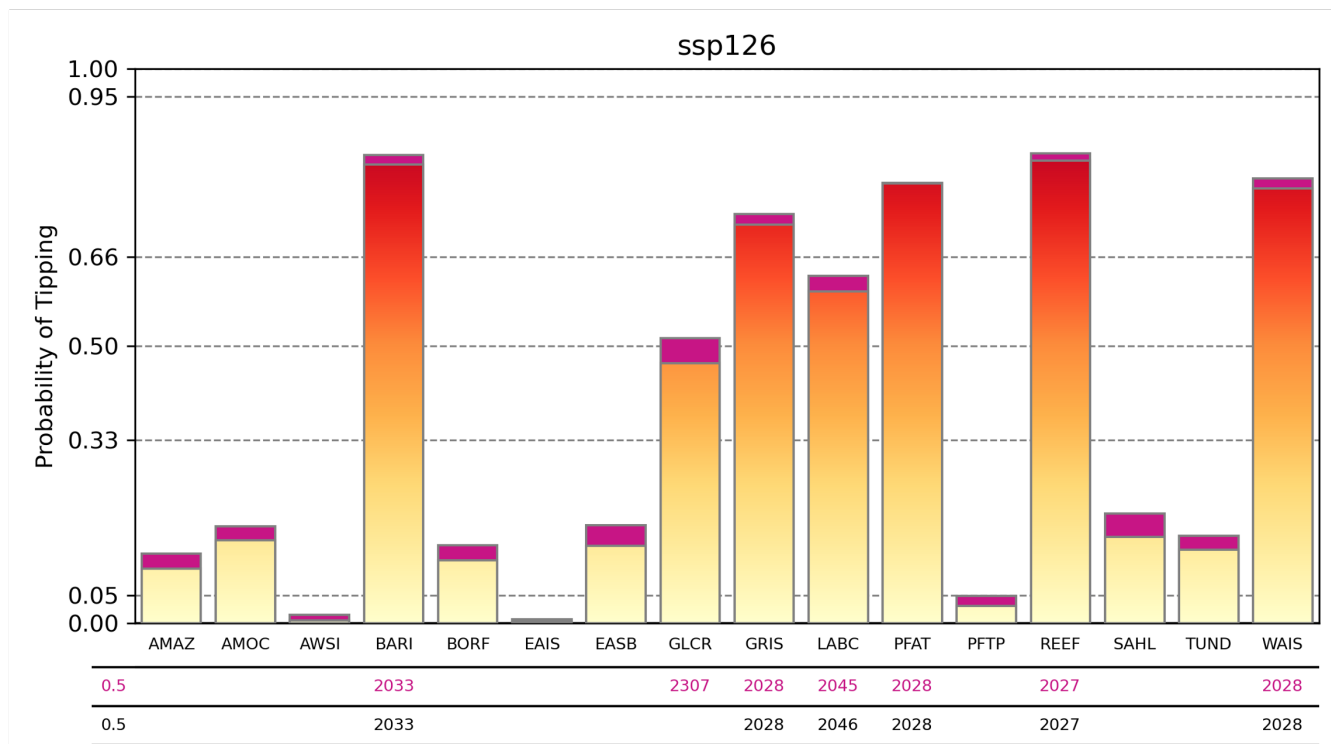
Figure 8. Probabilities of triggering the TEs by 2500 under SSP1-2.6. Additional probabilities from the carbon TEs are marked in purple. The table underneath states the years in which the 50% probability is crossed, with purple including carbon emissions from carbon TEs and black not.

carbon TEs, we calculate average triggering probabilities at the end of our model period in 2500 (Table 3). Unsurprisingly, they increase from ~~SSP1-1.9~~ SSP1-2.6 to SSP5-8.5.

Under SSP5-8.5, ~~triggering of most TEs becomes extremely likely~~ the probability of triggering is above 95% for most TEs, and only the probability for triggering EAIS ~~is remaining~~ remains just below 66% (Fig. 6). The probabilities of triggering

395 are reduced slightly under SSP3-7.0, but the general picture remains the same (Fig. ~~S11~~ S10). Interestingly, the additional probability of triggering TEs is lowest under the two high emission scenarios (Table 3). Temperatures well above the threshold temperatures of most TEs are reached even without the effect of carbon TEs, hence, their impact on triggering probabilities is almost negligible.

Under SSP2-4.5 the probabilities of triggering vary strongly between different TEs. The four TEs BARI, REEF, PFAT, and

400 WAIS are ~~extremely likely to be triggered~~ triggered with more than 95% probability under SSP2-4.5, with GRIS ~~and GLCR being extremely likely~~ crossing 95% probability as well if carbon emissions from carbon TEs are included (Fig. 7). GLCR, LABC, SAHL and, if carbon emissions from carbon TEs are included, EASB are ~~likely to be triggered~~ triggered with more than 66% probability. Additional carbon emissions from carbon TEs also lead to AMAZ and BORF becoming more likely than not to be triggered. Only AWSI, EAIS, and, if carbon emissions from carbon TEs are not accounted ~~, forPFTP remain unlikely~~

405 ~~to be~~ for, PFTP remain below 33% probability of getting triggered, as TUND and AMOC are exceeding 33% probability ~~of getting triggered~~ in both ensembles. Triggering of EAIS remains ~~extremely unlikely~~ below 5% probability only if carbon emissions from the carbon TEs are not included.

The increase in probabilities of triggering caused by carbon emissions from carbon TEs is highest under SSP2-4.5 (Table 3). This matches our finding that the highest long-term temperature increase from carbon TEs is also possible under this scenario
410 (Table 2). ~~Furthermore, GMST is generally increasing over time, which means that emissions from carbon TEs can produce temperature maxima when they occur, which is not the case for lower emission scenarios (Fig. 4).~~

Moving from SSP2-4.5 to SSP1-2.6 reduces the probability of triggering multiple TEs significantly, namely by ~~28~~27 pp (Table 3). No TE ~~is extremely likely to be~~ exceeds 95% probability of getting triggered under SSP1-2.6. However, the five TEs PFAT, REEF, GRIS, WAIS, and BARI are still ~~likely and LABC and GLCR are more likely than not to be triggered ,~~ triggered
415 with a probability higher than 66% regardless of carbon emissions from carbon TEs (Fig. 8). ~~All other TEs remain unlikely to be triggered, but only~~ The probability for triggering LABC is still higher than 50%, which is also true for GLCR if carbon emissions from carbon TEs are included. For all other TEs the probability of triggering remains below 33%, and even below 5% for AWSI, EAIS and PFTP ~~are extremely unlikely to be triggered~~ under SSP1-2.6. The additional probability of triggering from carbon TEs is also reduced by ~~one~~ 1.1 pp compared to SSP2-4.5 (Table 3).

420 ~~SSP1-1.9 represents the safest scenario with respect to triggering TEs. However, the reduction of triggering probabilities compared to SSP1-2.6 is comparably small, with only 11.2 pp (Table 3). Even under SSP1-1.9 the five TEs REEF, WAIS, PFAT, GRIS and BARI become more likely than not to be triggered until 2031, regardless of the temperature impact from carbon TEs (Fig. S12). REEF, WAIS, PFAT, and, if carbon emissions from carbon TEs are included, BARI even become likely to be triggered. This means that if the assumed TE temperature threshold distributions from Armstrong McKay et al. (2022)~~
425 ~~are accurate, it is already too late to steer the Earth towards a pathway that is safe with regard to triggering TEs.~~

6 Discussion

With CTEM we introduce a simplistic model which is able to represent carbon emissions from the three carbon TEs PFAT, PFTP and AMAZ in line with the estimates from Armstrong McKay et al. (2022). However, the impacts from the carbon TEs estimated in this study remain somewhat speculative, as there is only limited confidence about the actual existence of
430 tipping points within the carbon TEs, with low confidence for PFTP and medium confidence for PFAT and AMAZ (Table 1). The distinction between PFGT, PFAT and PFTP made by Armstrong McKay et al. (2022) for permafrost thaw also remains questionable. Most studies, including the latest IPCC report, assume that permafrost thaw can be divided into gradual and abrupt thaw processes, corresponding to PFGT and PFAT, and do not mention permafrost collapse due to compost bomb instabilities (PFTP) (e.g. Canadell et al., 2021; Turetsky et al., 2020; Schuur et al., 2015; Wang et al., 2023). Since PFTP
435 causes the highest carbon emissions out of all three carbon TEs with up to 250 GtC (Table 1), the impact of tipping elements within the carbon cycle will be less severe than found in this study if PFTP does not include a tipping point.

Yet, additional carbon emissions released by PFGT under continued global warming of up to 260 GtC (Table 1) need to be expected, which are not considered in this study. One reason to exclude PFGT is that it is not assumed to include tipping points, but to be a threshold-free feedback to global warming (Armstrong McKay et al., 2022). Furthermore, sophisticated models of

440 PFGT already exist (e.g. Gasser et al., 2018; Burke et al., 2020), hence it would not be appropriate to represent PFGT with a simple conceptual model like CTEM.

It is challenging to compare the carbon emissions from carbon TEs identified by us to other studies, as this is to the best of our knowledge the first study to investigate the impact of all TEs within the carbon cycle. Other studies are only analysing single TEs, e.g., Cox et al. (2004); Parry et al. (2022) for AMAZ or Schneider von Deimling et al. (2015); Gasser et al. (2018)

445 for permafrost thaw as a whole. Since the individual carbon emissions from the carbon TEs modelled by CTEM are based on the estimates of Armstrong McKay et al. (2022), we would only reproduce their analysis by comparing our individual carbon emission estimates to the literature. Nevertheless, it must be noted that even though the uncertainty ranges of the carbon impacts identified by Armstrong McKay et al. (2022) based on numerous studies are large (factor two for PFTP and AMAZ, factor three for PFAT), they do not include all estimates from the literature. Especially ~~,~~ the lower bounds of AMAZ and PFTP

450 are questionable. Carbon emissions from the Yedoma region, which make up for the major part of PFTP emissions, of only 23 GtC in 2300 under RCP5-8.5 have been found by an observations-based modelling study (Schneider von Deimling et al., 2015). This is much lower than the minimum carbon emissions of 100 GtC from the Yedoma region assumed by Armstrong McKay et al. (2022), which led to an estimated minimum impact of PFTP of 125 GtC. The minimum impact of 30 GtC for AMAZ might also be too high since no substantial carbon loss from AMAZ is observable in CMIP6 models, even if localized

455 dieback occurs (Parry et al., 2022).

~~A major shortcoming of CTEM is that it does not account for the temporal variability of the CH₄ emission fraction of PFAT and PFTP. However, we regard the temporal evolution of this fraction as too poorly constrained to be prescribed in CTEM since current model studies are rare and vary greatly (compare Turetsky et al. (2020) and Schneider von Deimling et al. (2015))~~ Given that the emission estimates from Armstrong McKay et al. (2022) used to parameterize CTEM seem to be on the high

460 side compared to other studies, we are confident about our finding that the warming caused by carbon TEs on average remains small compared to the anthropogenic warming.

Our estimates of probabilities of triggering are generally higher than the values reported by Kriegler et al. (2009), which have found much use in the climate tipping points literature (e.g. Lontzek et al., 2015; Cai et al., 2015, 2016). ~~There,~~ They provide ranges of probabilities of triggering ~~are provided~~ for the year 2200 under three warming scenarios: a low temperature

465 corridor comparable to SSP1-1.9, a medium temperature corridor comparable to SSP2-4.5 and a high temperature corridor comparable to SSP3-7.0. For the medium temperature corridor, Cai et al. (2016) infer mean probabilities of triggering from the ranges given in Kriegler et al. (2009) of 22% for AMOC, 52% for GRIS, 34% for WAIS, and 48% for AMAZ, which can be compared to our estimates in 2200 under SSP2-4.5 (without carbon TEs impacts) of 38% for AMOC, 94% for GRIS, 98% for WAIS, and 43% for AMAZ (Fig. ~~S15~~S12).

470 Those deviations can be explained by the new scientific literature being published since Kriegler et al. (2009), which ~~provide~~ provides the basis for the threshold temperature estimates from Armstrong McKay et al. (2022) ~~that~~ our calculation of triggering

probabilities is largely based on. The increased triggering probability for ~~the~~ AMOC can be linked to various studies reporting unrealistic stability of ~~the~~ AMOC in GCMs (e.g. Liu et al., 2017), together with empirical evidence for loss of stability of ~~the~~ AMOC (Boers, 2021). New indications for the proximity of a tipping point for GRIS are also derived from observations of ice loss (King et al., 2020; Boers and Rypdal, 2021), with recent modelling studies confirming this (Van Breedam et al., 2020; Robinson et al., 2012). Loss of WAIS is becoming observable (Shepherd et al., 2019) and a tipping point might already be crossed with several glaciers in the Amundsen Sea currently undergoing marine ice sheet instability (Rignot et al., 2014).

Even though we find an increase in the probabilities of triggering caused by the additional carbon emissions from carbon TEs, this impact is not strong enough to trigger any tipping cascades and remains small compared to the scenario–dependence of tipping probabilities. Additional carbon emissions from carbon TEs only cause existing clusters of TEs to be triggered earlier ~~. They do not produce any additional clusters of triggering~~ (Fig. 5). Even under SSP2-4.5, which features the highest long-term increase in temperature of up to 0.91°C due to carbon emissions from carbon TEs, the additional probability of triggering caused by this temperature increase is only 3.3 pp on average and only two TEs become more likely than not to be triggered if this temperature increase is accounted for. Despite our finding that the impact from carbon TEs alone is too small to trigger tipping cascades, tipping cascades might still emerge as major physical interactions between TEs aside from carbon emissions are not accounted for in this study (Wunderling et al., 2021).

A shortcoming of our calculation of triggering probabilities is that we do not allow for temporal overshoot of threshold temperatures but count a tipping element as triggered once its threshold temperature is crossed. For how long the threshold temperature can be exceeded without triggering depends on the internal timescale of the TE, and is therefore especially pronounced for TEs within the cryosphere (Ritchie et al., 2021). Therefore, we might be overestimating probabilities of triggering for cryospheric TEs under SSP1-2.6, which features a slight temperature overshoot. Further constraining the internal timescales of TEs could be an interesting topic of future research and would enable studies like ours to include the possibility for overshoot.

~~Our work indicates that the pathway the world is currently on, which is comparable to SSP2-4.5 (Climate Action Tracker, 2022), is highly unsafe with regard to triggering~~ It must also be noted that our findings critically depend on the assessment of climate tipping points by Armstrong McKay et al. (2022). However, we believe that this study best summarizes the current state of knowledge about climate tipping points ~~There is deep uncertainty about the~~, relying on more than 300 references. Narrowing the uncertainty range of threshold temperatures is an enormous task for future research, which would allow for more precise statements about the probability of triggering climate TEs.

7 Conclusions

We developed a simple model framework to explore the probabilities of triggering climate TEs and how they are amplified by carbon emissions from carbon TEs under ~~this scenario, but the highest additional long-term temperature increase of all SSPs becomes possible, with the additional warming in 2500 ranging from 0.03°C to 0.91°C (5th to 95th percentile). Temperature impacts from carbon TEs can be especially high under SSP2-4.5 since maximum carbon emissions~~ various SSPs.

We show that the additional carbon emissions from carbon TEs increase the risk for high temperature pathways, especially under SSPs with comparably low anthropogenic carbon emissions. On average, however, the additional warming from carbon TEs remains low compared to the anthropogenic warming. Therefore, the probability of triggering climate TEs is to first order determined by the emission scenario and not by whether carbon TEs are triggered or not. Consistent with this, we also don't see any tipping cascades being triggered by carbon TEs.

Current policies, steering towards a pathway comparable to SSP2-4.5 (Climate Action Tracker, 2022; United Nations Environment Programme, are highly unsafe with regard to triggering climate tipping points. Triggering of multiple TEs is likely under SSP2-4.5 with 64% probability of triggering on average over all 16 TEs in 2500. The temperature increase from carbon TEs increases this number by 3.3 pp, which is the highest probability increase caused by carbon TEs among all SSPs.

This is in line with the highest long-term temperature increase caused by carbon TEs becoming possible under SSP2-4.5, with values reaching from 0.03°C to 0.91°C in 2500 (5th to 95th percentile range). Moving from SSP2-4.5 to SSP1-2.6 reduces the probability of triggering TEs substantially, with an average probability of triggering until 2500 of 37% under SSP1-2.6. The impact of carbon TEs is also less severe under this scenario, ranging from 0°C to 0.54°C in 2500, which leads to an increase in the average probability of triggering of 2.2 pp.

The probabilities of triggering climate TEs derived by us are higher than the estimates from the often cited expert elicitation conducted by (Kriegler et al., 2009). This is explained by recent evidence for the proximity of climate tipping points, leading to low estimates of the respective threshold temperatures.

If the risk of triggering TEs is to be reduced, rapid action is needed to reduce greenhouse gas emissions, since climate tipping points are already close, and it will be decided within the coming decades if they will be crossed or not.

Code and data availability. The code to reproduce the model output and the plots is available from https://github.com/JakobDeutloff/TP_paper and archived under https://zenodo.org/records/10136536 (Deutloff, 2023b). The model output and the parameter sets used to produce it are archived under https://zenodo.org/records/10136870 (Deutloff, 2023a).

Author contributions. JD designed the study and wrote the paper with input from both co-authors. JD performed and analysed the model simulations and prepared all figures and tables. HH co-designed the sampling strategy, and contributed to the discussion of the method and the results. TL contributed to the research design and the discussion of the methods and the results.

540   *Competing interests.* Tim Lenton is an editor of the special issue on tipping points in the Anthropocene. The peer-review process was guided by an independent editor, and the authors have also no other competing interests to declare.

Acknowledgements. The authors would like to thank David Armstrong McKay and Jesse Abrams for the discussion of ideas and valuable suggestions for the model development. The Global Systems Institute, where the major part of this research was conducted, was supported by the Bezos Earth Fund.

545 References

Armstrong McKay, D. I., Staal, A., Abrams, J. F., Winkelmann, R., Sakschewski, B., Loriani, S., Fetzer, I., Cornell, S. E., Rockström, J., and Lenton, T. M.: Exceeding 1.5°C global warming could trigger multiple climate tipping points, Science (New York, N.Y.), 377, eabn7950, https://doi.org/10.1126/science.abn7950, 2022.

Belgorodski, N., Greiner, M., Tolksdorf, K., Schueller, K., Flor, M., and Göhring, L.: rriskDistributions, https://CRAN.R-project.org/package=rriskDistributions, 2017.

550

Boers, N.: Observation-based early-warning signals for a collapse of the Atlantic Meridional Overturning Circulation, Nature Climate Change, 11, 680–688, https://doi.org/10.1038/s41558-021-01097-4, 2021.

Boers, N. and Rypdal, M.: Critical slowing down suggests that the western Greenland Ice Sheet is close to a tipping point, Proceedings of the National Academy of Sciences of the United States of America, 118, 1–7, https://doi.org/10.1073/pnas.2024192118, 2021.

555 Burke, E. J., Zhang, Y., and Krinner, G.: Evaluating permafrost physics in the Coupled Model Intercomparison Project 6 (CMIP6) models and their sensitivity to climate change, Cryosphere, 14, 3155–3174, https://doi.org/10.5194/tc-14-3155-2020, 2020.

Cai, Y., Judd, K. L., Lenton, T. M., Lontzek, T. S., and Narita, D.: Environmental tipping points significantly affect the cost-benefit assessment of climate policies, Proceedings of the National Academy of Sciences, 112, 4606–4611, https://doi.org/10.1073/pnas.1503890112, 2015.

Cai, Y., Lenton, T. M., and Lontzek, T. S.: Risk of multiple interacting tipping points should encourage rapid CO2 emission reduction, Nature

560 Climate Change, 6, 520–525, https://doi.org/10.1038/nclimate2964, 2016.

Canadell, J., Monteiro, P., Costa, M., Cotrim da Cunha, L., Cox, P., Eliseev, A., Henson, S., Ishii, M., Jaccard, S., Koven, C., Lohila, A., Patra, P., Piao, S., Rogelj, J., Syampungani, S., Zaehle, S., and Zickfeld, K.: Global Carbon and other Biogeochemical Cycles and Feedbacks, in: Climate Change 2021: The Physical Science Basis. Contribution of Working Group I to the Sixth Assessment Report of the Intergovernmental Panel on Climate Change, edited by Masson-Delmotte, V., Zhai, P., Pirani, A., Connors, S., Péan, C.,

565 Berger, S., Caud, N., Chen, Y., Goldfarb, L., Gomis, M., Huang, M., Leitzell, K., Lonnoy, E., Matthews, J., Maycock, T., Waterfield, T., Yelekçi, O., Yu, R., and Zhou, B., p. 673–816, Cambridge University Press, Cambridge, United Kingdom and New York, NY, USA, https://doi.org/10.1017/9781009157896.007, 2021.

Chen, D., Rojas, M., Samset, B., Cobb, K., Diongue Niang, A., Edwards, P., Emori, S., Faria, S., Hawkins, E., Hope, P., Huybrechts, P., Meinshausen, M., Mustafa, S., Plattner, G.-K., and Tréguier, A.-M.: Framing, Context, and Methods, in: Climate Change 2021: The

570 Physical Science Basis. Contribution of Working Group I to the Sixth Assessment Report of the Intergovernmental Panel on Climate Change, edited by Masson-Delmotte, V., Zhai, P., Pirani, A., Connors, S., Péan, C., Berger, S., Caud, N., Chen, Y., Goldfarb, L., Gomis, M., Huang, M., Leitzell, K., Lonnoy, E., Matthews, J., Maycock, T., Waterfield, T., Yelekçi, O., Yu, R., and Zhou, B., p. 147–286, Cambridge University Press, Cambridge, United Kingdom and New York, NY, USA, https://doi.org/10.1017/9781009157896.003, 2021.

Climate Action Tracker: The CAT Thermometer, https://climateactiontracker.org/global/cat-thermometer/, 2022.

575 Cox, P. M., Betts, R. A., Collins, M., Harris, P. P., Huntingford, C., and Jones, C. D.: Amazonian forest dieback under climate-carbon cycle projections for the 21st century, Theoretical and Applied Climatology, 78, 137–156, https://doi.org/10.1007/s00704-004-0049-4, 2004.

Deutloff, J.: Ensemble Outputs and Triggering Probabilities (Dataset), https://doi.org/10.5281/zenodo.8099908, 2023a.

Deutloff, J.: Model Code and Evaluation Scripts (Version 1.1), https://doi.org/10.5281/zenodo.8121160, 2023b.

Etminan, M., Myhre, G., Highwood, E. J., and Shine, K. P.: Radiative forcing of carbon dioxide, methane, and nitrous oxide: A signifi-

580 cant revision of the methane radiative forcing, Geophysical Research Letters, 43, 12,614–12,623, https://doi.org/10.1002/2016GL071930, _eprint: https://onlinelibrary.wiley.com/doi/pdf/10.1002/2016GL071930, 2016.

Forster, P., Storelvmo, T., Armour, K., Collins, W., Dufresne, J.-L., Frame, D., Lunt, D., Mauritsen, T., Palmer, M., Watanabe, M., Wild, M., and Zhang, H.: The Earth's Energy Budget, Climate Feedbacks, and Climate Sensitivity, in: Climate Change 2021: The Physical Science Basis. Contribution of Working Group I to the Sixth Assessment Report of the Intergovernmental Panel on Climate Change, edited by
585   Masson-Delmotte, V., Zhai, P., Pirani, A., Connors, S., Péan, C., Berger, S., Caud, N., Chen, Y., Goldfarb, L., Gomis, M., Huang, M., Leitzell, K., Lonnoy, E., Matthews, J., Maycock, T., Waterfield, T., Yelekçi, O., Yu, R., and Zhou, B., p. 923–1054, Cambridge University Press, Cambridge, United Kingdom and New York, NY, USA, https://doi.org/10.1017/9781009157896.009, 2021.

Gasser, T., Kechiar, M., Ciais, P., Burke, E. J., Kleinen, T., Zhu, D., Huang, Y., Ekici, A., and Obersteiner, M.: Path-dependent reductions in CO_2 emission budgets caused by permafrost carbon release, Nature Geoscience, 11, 830–835, https://doi.org/10.1038/s41561-018-0227-0,
590   2018.

Gidden, M. J., Riahi, K., Smith, S. J., Fujimori, S., Luderer, G., Kriegler, E., Van Vuuren, D. P., Van Den Berg, M., Feng, L., Klein, D., Calvin, K., Doelman, J. C., Frank, S., Fricko, O., Harmsen, M., Hasegawa, T., Havlik, P., Hilaire, J., Hoesly, R., Horing, J., Popp, A., Stehfest, E., and Takahashi, K.: Global emissions pathways under different socioeconomic scenarios for use in CMIP6: A dataset of harmonized emissions trajectories through the end of the century, Geoscientific Model Development, 12, 1443–1475, https://doi.org/10.5194/gmd-12-
595   1443-2019, 2019.

Guetschow, J., Jeffery, M. L., Gieseke, R., Gebel, R., Stevens, D., Krapp, M., and Rocha, M.: The PRIMAP-hist national historical emissions time series, Earth System Science Data, 8, 571–603, https://doi.org/10.5194/essd-8-571-2016, 2016.

Hoesly, R. M., Smith, S. J., Feng, L., Klimont, Z., Janssens-Maenhout, G., Pitkanen, T., Seibert, J. J., Vu, L., Andres, R. J., Bolt, R. M., Bond, T. C., Dawidowski, L., Kholod, N., Kurokawa, J.-I., Li, M., Liu, L., Lu, Z., Moura, M. C. P., O'Rourke, P. R., and Zhang, Q.: Historical
600   (1750–2014) anthropogenic emissions of reactive gases and aerosols from the Community Emissions Data System (CEDS), Geoscientific Model Development, 11, 369–408, https://doi.org/10.5194/gmd-11-369-2018, 2018.

IPCC: Summary for Policymakers, p. 3-32, Cambridge University Press, Cambridge, United Kingdom and New York, NY, USA, https://doi.org/10.1017/9781009157896.001, 2021.

Jewell, J. and Cherp, A.: On the political feasibility of climate change mitigation pathways: Is it too late to keep warming below 1.5°C?,
605   WIREs Climate Change, 11, https://doi.org/10.1002/wcc.621, 2020.

Khvorostyanov, D. V., Ciais, P., Krinner, G., and Zimov, S. A.: Vulnerability of east Siberia's frozen carbon stores to future warming, Geophysical Research Letters, 35, 1–5, https://doi.org/10.1029/2008GL033639, 2008.

King, M. D., Howat, I. M., Candela, S. G., Noh, M. J., Jeong, S., Noël, B. P. Y., van den Broeke, M. R., Wouters, B., and Negrete, A.: Dynamic ice loss from the Greenland Ice Sheet driven by sustained glacier retreat, Communications Earth & Environment, 1, 1,
610   https://doi.org/10.1038/s43247-020-0001-2, 2020.

Kriegler, E., Hall, J. W., Held, H., Dawson, R., and Schellnhuber, H. J.: Imprecise probability assessment of tipping points in the climate system, Proceedings of the National Academy of Sciences of the United States of America, 106, 5041–5046, https://doi.org/10.1073/pnas.0809117106, 2009.

Le Quéré, C., Andrew, R. M., Canadell, J. G., Sitch, S., Ivar Korsbakken, J., Peters, G. P., Manning, A. C., Boden, T. A., Tans, P. P., Houghton,
615   R. A., Keeling, R. F., Alin, S., Andrews, O. D., Anthoni, P., Barbero, L., Bopp, L., Chevallier, F., Chini, L. P., Ciais, P., Currie, K., Delire, C., Doney, S. C., Friedlingstein, P., Gkritzalis, T., Harris, I., Hauck, J., Haverd, V., Hoppema, M., Klein Goldewijk, K., Jain, A. K., Kato, E., Körtzinger, A., Landschützer, P., Lefèvre, N., Lenton, A., Lienert, S., Lombardozzi, D., Melton, J. R., Metzl, N., Millero, F., Monteiro, P. M., Munro, D. R., Nabel, J. E., Nakaoka, S. I., O'Brien, K., Olsen, A., Omar, A. M., Ono, T., Pierrot, D., Poulter, B., Rödenbeck, C., Salisbury, J., Schuster, U., Schwinger, J., Séférian, R., Skjelvan, I., Stocker, B. D., Sutton, A. J., Takahashi, T., Tian, H., Tilbrook, B., Van

620   Der Laan-Luijkx, I. T., Van Der Werf, G. R., Viovy, N., Walker, A. P., Wiltshire, A. J., and Zaehle, S.: Global Carbon Budget 2016, Earth System Science Data, 8, 605–649, https://doi.org/10.5194/essd-8-605-2016, 2016.

Leach, N. J., Jenkins, S., Nicholls, Z., Smith, C. J., Lynch, J., Cain, M., Walsh, T., Wu, B., Tsutsui, J., and Allen, M. R.: FaIRv2.0.0: A generalized impulse response model for climate uncertainty and future scenario exploration, Geoscientific Model Development, 14, 3007–3036, https://doi.org/10.5194/gmd-14-3007-2021, 2021.

625   Lee, J.-Y., Marotzke, J., Bala, G., Cao, L., Corti, S., Dunne, J., Engelbrecht, F., Fischer, E., Fyfe, J., Jones, C., Maycock, A., Mutemi, J., Ndiaye, O., Panickal, S., and Zhou, T.: Future Global Climate: Scenario-Based Projections and Near-Term Information, in: Climate Change 2021: The Physical Science Basis. Contribution of Working Group I to the Sixth Assessment Report of the Intergovernmental Panel on Climate Change, edited by Masson-Delmotte, V., Zhai, P., Pirani, A., Connors, S., Péan, C., Berger, S., Caud, N., Chen, Y., Goldfarb, L., Gomis, M., Huang, M., Leitzell, K., Lonnoy, E., Matthews, J., Maycock, T., Waterfield, T., Yelekçi, O., Yu, R., and Zhou, B., p. 553–672,
630   Cambridge University Press, Cambridge, United Kingdom and New York, NY, USA, https://doi.org/10.1017/9781009157896.006, 2021.

Lenton, T. M., Held, H., Kriegler, E., Hall, J. W., Lucht, W., Rahmstorf, S., and Schellnhuber, H. J.: Tipping elements in the Earth's climate system, Proceedings of the National Academy of Sciences, 105, 1786–1793, https://doi.org/10.1073/pnas.0705414105, 2008.

Lenton, T. M., Rockström, J., Gaffney, O., Rahmstorf, S., Richardson, K., Steffen, W., and Schellnhuber, H. J.: Climate tipping points — too risky to bet against, Nature, 575, 592–595, 2019.

635   Liu, W., Xie, S.-P., Liu, Z., and Zhu, J.: Overlooked possibility of a collapsed Atlantic Meridional Overturning Circulation in warming climate, Science Advances, 3, e1601 666, https://doi.org/10.1126/sciadv.1601666, 2017.

Lontzek, T. S., Cai, Y., Judd, K. L., and Lenton, T. M.: Stochastic integrated assessment of climate tipping points indicates the need for strict climate policy, Nature Climate Change, 5, 441–444, https://doi.org/10.1038/nclimate2570, 2015.

Luke, C. M. and Cox, P. M.: Soil carbon and climate change: From the Jenkinson effect to the compost-bomb instability, European Journal
640   of Soil Science, 62, 5–12, https://doi.org/10.1111/j.1365-2389.2010.01312.x, 2011.

McKay, M. D., Beckman, R. J., and Conover, W. J.: A Comparison of Three Methods for Selecting Values of Input Variables in the Analysis of Output from a Computer Code, Technometrics, 21, 239–245, https://doi.org/10.2307/1268522, publisher: [Taylor & Francis, Ltd., American Statistical Association, American Society for Quality], 1979.

Meinshausen, M., Nicholls, Z. R., Lewis, J., Gidden, M. J., Vogel, E., Freund, M., Beyerle, U., Gessner, C., Nauels, A., Bauer, N., Canadell,
645   J. G., Daniel, J. S., John, A., Krummel, P. B., Luderer, G., Meinshausen, N., Montzka, S. A., Rayner, P. J., Reimann, S., Smith, S. J., Van Den Berg, M., Velders, G. J., Vollmer, M. K., and Wang, R. H.: The shared socio-economic pathway (SSP) greenhouse gas concentrations and their extensions to 2500, Geoscientific Model Development, 13, 3571–3605, https://doi.org/10.5194/gmd-13-3571-2020, 2020.

Meinshausen, M., Lewis, J., McGlade, C., Gütschow, J., Nicholls, Z., Burdon, R., Cozzi, L., and Hackmann, B.: Realization of Paris Agreement pledges may limit warming just below 2 °C, Nature, 604, 304–309, https://doi.org/10.1038/s41586-022-04553-z, 2022.

650   Metropolis, N., Rosenbluth, A. W., Rosenbluth, M. N., Teller, A. H., and Teller, E.: Equation of State Calculations by Fast Computing Machines, The Journal of Chemical Physics, 21, 1087–1092, https://doi.org/10.1063/1.1699114, 1953.

Myhre, G.and Shindell, D., Bréon, F.-M., Collins, W.and Fuglestvedt, J., Huang, J., Koch, D., Lamarque, J.-F., Lee, D.and Mendoza, B., Nakajima, T.and Robock, A., Stephens, G., Takemura, T., and Zhang, H.: Anthropogenic and Natural Radiative Forcing, in: Climate Change 2013: The Physical Science Basis. Contribution of Working Group I to the Fifth Assessment Report of the Intergovernmental
655   Panel on Climate Change, edited by Stocker, T. F., Qin, D., Plattner, G.-K., Tignor, M., Allen, S. K., Boschung, J., Nauels, A., Xia, Y., Bex, V., and Midgley, P. M., chap. 8, pp. 650–740, Cambridge University Press, Cambridge, United Kingdom and New York, NY, USA, https://doi.org/10.1017/CBO9781107415324.018, 2013.

Nicholls, Z. R. J., Meinshausen, M., Lewis, J., Gieseke, R., Dommenget, D., Dorheim, K., Fan, C.-S., Fuglestvedt, J. S., Gasser, T., Golueke, U., Goodwin, P., Hartin, C., Hope, A. P., Kriegler, E., Leach, N. J., Marchegiani, D., McBride, L. A., Quilcaille, Y., Rogelj, J., Salawitch, R. J., Samset, B. H., Sandstad, M., Shiklomanov, A. N., Skeie, R. B., Smith, C. J., Smith, S., Tanaka, K., Tsutsui, J., and Xie, Z.: Reduced Complexity Model Intercomparison Project Phase 1: introduction and evaluation of global-mean temperature response, Geoscientific Model Development, 13, 5175–5190, https://doi.org/10.5194/gmd-13-5175-2020, 2020.

Nobre, C. A., Sampaio, G., Borma, L. S., Castilla-Rubio, J. C., Silva, J. S., and Cardoso, M.: Land-use and climate change risks in the amazon and the need of a novel sustainable development paradigm, Proceedings of the National Academy of Sciences of the United States of America, 113, 10 759–10 768, https://doi.org/10.1073/pnas.1605516113, 2016.

Olefeldt, D., Goswami, S., Grosse, G., Hayes, D., Hugelius, G., Kuhry, P., Mcguire, A. D., Romanovsky, V. E., Sannel, A. B., Schuur, E. A., and Turetsky, M. R.: Circumpolar distribution and carbon storage of thermokarst landscapes, Nature Communications, 7, 1–11, https://doi.org/10.1038/ncomms13043, 2016.

O'Neill, B. C., Tebaldi, C., Van Vuuren, D. P., Eyring, V., Friedlingstein, P., Hurtt, G., Knutti, R., Kriegler, E., Lamarque, J. F., Lowe, J., Meehl, G. A., Moss, R., Riahi, K., and Sanderson, B. M.: The Scenario Model Intercomparison Project (ScenarioMIP) for CMIP6, Geoscientific Model Development, 9, 3461–3482, https://doi.org/10.5194/gmd-9-3461-2016, 2016.

Parry, I., Ritchie, P., and Cox, P.: Evidence of Amazon rainforest dieback in CMIP6 models, EGUsphere, pp. 1–11, http://arxiv.org/abs/2203.11744, 2022.

Rignot, E., Mouginot, J., Morlighem, M., Seroussi, H., and Scheuchl, B.: Widespread, rapid grounding line retreat of Pine Island, Thwaites, Smith, and Kohler glaciers, West Antarctica, from 1992 to 2011, Geophysical Research Letters, 41, 3502–3509, https://doi.org/10.1002/2014GL060140, 2014.

Ritchie, P. D., Clarke, J. J., Cox, P. M., and Huntingford, C.: Overshooting tipping point thresholds in a changing climate, Nature, 592, 517–523, https://doi.org/10.1038/s41586-021-03263-2, publisher: Springer US, 2021.

Robinson, A., Calov, R., and Ganopolski, A.: Multistability and critical thresholds of the Greenland ice sheet, Nature Climate Change, 2, 429–432, https://doi.org/10.1038/nclimate1449, 2012.

Schneider von Deimling, T., Grosse, G., Strauss, J., Schirrmeister, L., Morgenstern, A., Schaphoff, S., Meinshausen, M., and Boike, J.: Observation-based modelling of permafrost carbon fluxes with accounting for deep carbon deposits and thermokarst activity, Biogeosciences, 12, 3469–3488, https://doi.org/10.5194/bg-12-3469-2015, 2015.

Schuur, E. A., McGuire, A. D., Schädel, C., Grosse, G., Harden, J. W., Hayes, D. J., Hugelius, G., Koven, C. D., Kuhry, P., Lawrence, D. M., Natali, S. M., Olefeldt, D., Romanovsky, V. E., Schaefer, K., Turetsky, M. R., Treat, C. C., and Vonk, J. E.: Climate change and the permafrost carbon feedback, Nature, 520, 171–179, https://doi.org/10.1038/nature14338, 2015.

Science Panel for the Amazon: Executive Summary, in: Science Panel for the Amazon Amazon Assessment Report 2021, edited by Nobre, C., Encalada, A., Anderson, E., Roca Alcazar, F., Bustamante, M., Mena, C., Peña-Claros, M., Poveda, G., Rodriguez, J., Saleska, S., Trumbore, S., Val, A., Nova, L. V., Abramovay, R., Alencar, A., Alzza, A., Armenteras, D., Artaxo, P., Athayde, S., Barretto Filho, H., Barlow, J., Berenguer, E., Bortolotto, F., Costa, F., Costa, M., Cuvi, N., Fearnside, P., Ferreira, J., Flores, B., Frieri, S., Gatti, L., Guayasamin, J., Hecht, S., Hirota, M., Hoorn, C., Josse, C., Lapola, D., Larrea, C., Larrea-Alcazar, D., Lehm Ardaya, Z., Malhi, Y., Marengo, J., Moraes, M., Moutinho, P., Murmis, M., Neves, E., Paez, B., Painter, L., Ramos, A., Rosero-Peña, M., Schmink, M., Sist, P., Ter Steege, H., Val, P., Van der Voort, H., Varese, M., and Zapata-Ríos, p. 48, United Nations Sustainable Development Solutions Network, New York, 2021.

695 Shepherd, A., Gilbert, L., Muir, A. S., Konrad, H., McMillan, M., Slater, T., Briggs, K. H., Sundal, A. V., Hogg, A. E., and Engdahl, M. E.: Trends in Antarctic Ice Sheet Elevation and Mass, Geophysical Research Letters, 46, 8174–8183, https://doi.org/10.1029/2019GL082182, 2019.

Smith, C. J.: Effective Radiative Forcing Time Series from the Shared Socioeconomic Pathways, https://doi.org/10.5281/zenodo.3973015, 2020.

700 Steffen, W., Rockström, J., Richardson, K., Lenton, T. M., Folke, C., Liverman, D., Summerhayes, C. P., Barnosky, A. D., Cornell, S. E., Crucifix, M., Donges, J. F., Fetzer, I., Lade, S. J., Scheffer, M., Winkelmann, R., and Schellnhuber, H. J.: Trajectories of the Earth System in the Anthropocene, https://doi.org/10.1073/pnas.1810141115, 2018.

Turetsky, M. R., Abbott, B. W., Jones, M. C., Anthony, K. W., Olefeldt, D., Schuur, E. A. G., Koven, C., McGuire, A. D., Grosse, G., Kuhry, P., Hugelius, G., Lawrence, D. M., Gibson, C., and Sannel, A. B. K.: Permafrost collapse is accelerating carbon release, Nature, pp. 32–34,
705 https://www.nature.com/articles/d41586-019-01313-4, 2019.

Turetsky, M. R., Abbott, B. W., Jones, M. C., Anthony, K. W., Olefeldt, D., Schuur, E. A., Grosse, G., Kuhry, P., Hugelius, G., Koven, C., Lawrence, D. M., Gibson, C., Sannel, A. B. K., and McGuire, A. D.: Carbon release through abrupt permafrost thaw, Nature Geoscience, 13, 138–143, https://doi.org/10.1038/s41561-019-0526-0, 2020.

United Nations Environment Programme: Emissions Gap Report 2022: The Closing Window — Climate crisis calls for rapid transformation
710 of societies, https://www.unep.org/resources/emissions-gap-report-2022, 2022.

Van Breedam, J., Goelzer, H., and Huybrechts, P.: Semi-equilibrated global sea-level change projections for the next 10 000 years, Earth System Dynamics, 11, 953–976, https://doi.org/10.5194/esd-11-953-2020, 2020.

Van Marle, M. J., Kloster, S., Magi, B. I., Marlon, J. R., Daniau, A. L., Field, R. D., Arneth, A., Forrest, M., Hantson, S., Kehrwald, N. M., Knorr, W., Lasslop, G., Li, F., Mangeon, S., Yue, C., Kaiser, J. W., and Van Der Werf, G. R.: Historic global biomass burning emissions for
715 CMIP6 (BB4CMIP) based on merging satellite observations with proxies and fire models (1750-2015), Geoscientific Model Development, 10, 3329–3357, https://doi.org/10.5194/gmd-10-3329-2017, 2017.

Wang, S., Foster, A., Lenz, E. A., Kessler, J. D., Stroeve, J. C., Anderson, L. O., Turetsky, M., Betts, R., Zou, S., Liu, W., Boos, W. R., and Hausfather, Z.: Mechanisms and Impacts of Earth System Tipping Elements, Reviews of Geophysics, 61, https://doi.org/10.1029/2021RG000757, 2023.

720 Wunderling, N., Donges, J. F., Kurths, J., and Winkelmann, R.: Interacting tipping elements increase risk of climate domino effects under global warming, Earth System Dynamics, 12, 601–619, https://doi.org/10.5194/esd-12-601-2021, 2021.